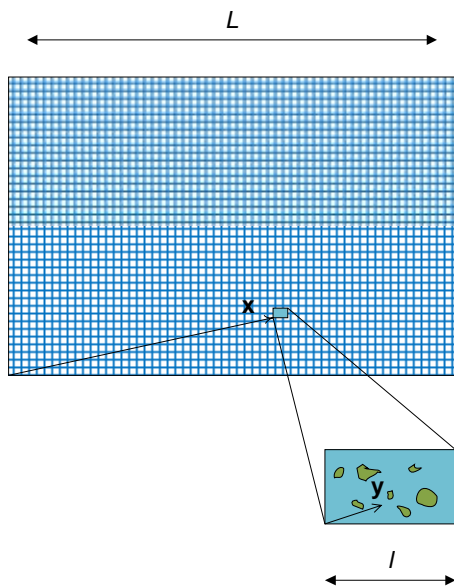


## RESEARCH REPORT


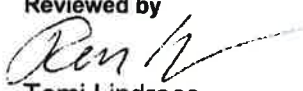

VTT-R-05212-16



# Multi-scale computation of sound absorbing materials

Author: Seppo Uosukainen

Confidentiality: Public

<b>Report's title</b>	
Multi-scale computation of sound absorbing materials	
<b>Customer, contact person, address</b>	<b>Order reference</b>
FIMECC Ltd. / Tekes	
<b>Project name</b>	<b>Project number/Short name</b>
FIMECC/HYBRIDS/IND/2016 - P3 SP3	110035 – 1.3.1
<b>Author(s)</b>	<b>Pages</b>
Seppo Uosukainen	43
<b>Keywords</b>	<b>Report identification code</b>
permeability, tortuosity, characteristic lengths	VTT-R-05212-16
<b>Summary</b>	
<p>The multi-scale computation method has been treated for acoustical purposes, for controlling the chain of parameters including the relations between the microscopic, macroscopic and acoustic parameters of sound absorbing materials. Possible anisotropic behaviour of materials has been taken into account.</p> <p>The macro-scale parameters complex density and complex compressibility are produced by the multi-scale computation. Their imaginary parts are due to the viscous and thermal losses of the fluid in porous materials. The deviations of their real parts from their physical values take into account some other things affecting the sound propagation in porous materials.</p> <p>The macro-scale complex parameters can be defined using two alternative ways: the direct numerical approach and the hybrid numerical approach. In the former, the complex density and compressibility are directly formed from the calculated dynamic viscous and thermal permeability functions. In the latter, static viscous and thermal permeability functions, three tortuosity functions (the strict amount depending on the selection from three possible models), and the viscous and thermal characteristic lengths, are computed, from which the complex density and compressibility are finally calculated. From the complex density and compressibility, the impedance and the complex wave number for rigid frame models are computed similarly in both of the methods. In the Biot model, the viscous and thermal effects are coupled, so the logic presented for the rigid frame models cannot be directly. However, the effective compressibility and the dynamic viscous tortuosity, based on either of the approaches, can directly be included in the parameters of the Biot model, to take into account the viscous and thermal properties of the fluid phase.</p>	
<b>Confidentiality</b>	Public
Espoo, 30.11.2016	
<b>Written by</b>	<b>Reviewed by</b>
	
Seppo Uosukainen Principal Scientist	Tomi Lindroos Research Team Leader
	<b>Accepted by</b>
	
	Johannes Hyrynen Vice President
<b>VTT's contact address</b>	
Seppo Uosukainen, P.O. Box 1000, FI-02044 VTT, Finland	
<b>Distribution (customer and VTT)</b>	
Customer 1 copy (electronic) VTT 1 copy	
<p><i>The use of the name of VTT Technical Research Centre of Finland Ltd in advertising or publishing of a part of this report is only permissible with written authorisation from VTT Technical Research Centre of Finland Ltd.</i></p>	

## Preface

---

The work described in this report has been carried out in VTT Efficient Machines and Vehicles, Structural Dynamics and Vibroacoustics Team. The results were obtained through Task 1 (Noise and Vibration Control through Multifunctional Low Weight Hybrid Structures) of Subproject 1 (Design and Manufacturing of Functional Sandwich and Reinforced Composite Structures) of Project 3 (Light Multifunctional Hybrid Structures) in the HYBRIDS programme (Hybrid Materials) of FIMECC SHOK with funding from Tekes. The aim of this report is to give a thorough presentation of the multi-scale computation method for acoustical purposes.

Espoo 30.11.2016

Author

## Contents

---

Preface.....	2
Contents.....	3
1. Introduction.....	4
2. Goal.....	4
3. Models for absorptive materials.....	5
4. Basics of multi-scale computation of sound absorbing materials.....	6
4.1 Periodic structures.....	6
4.2 Preliminaries in multi-scale computation.....	7
4.3 Multi-scale methods.....	7
4.3.1 Direct numerical approach.....	10
4.3.2 Hybrid numerical approach.....	10
4.3.3 Extension to Biot model.....	11
5. Typical results found with multi-scale computation.....	11
6. Basic field equations.....	13
7. Multi-scale asymptotic method.....	14
7.1 Power series in multi-scale method.....	15
7.2 Power series of basic field equations.....	15
7.3 Equations of multi-scale method for sound absorbing materials.....	16
8. Homogenized macro-scale parameters.....	18
8.1 Direct numerical approach.....	18
8.1.1 Effective density.....	19
8.1.2 Dynamic viscous tortuosity.....	19
8.1.3 Effective compressibility.....	19
8.1.4 Dynamic thermal tortuosity.....	21
8.1.5 Effective sound speed and characteristic impedance in rigid frame models.....	21
8.2 Hybrid numerical approach.....	21
8.2.1 Viscous relaxed tortuosity $\alpha_0$ .....	23
8.2.2 Thermal relaxed tortuosity $\alpha'_0$ .....	25
8.2.3 Viscous tortuosity $\alpha_\infty$ .....	26
8.2.4 Thermal tortuosity $\alpha'_\infty$ .....	27
8.2.5 Viscous characteristic length.....	28
8.2.6 Thermal characteristic length.....	31
8.2.7 Dynamic tortuosity and compressibility.....	31
9. Biot model.....	34
9.1 Stress-strain relationships.....	34
9.2 Equations of motion.....	35
9.3 Biot equations.....	35
9.4 Compressional waves.....	37
9.4.1 Wave numbers.....	37
9.4.2 Displacement relationships.....	38
9.4.3 Characteristic impedances.....	39
9.5 Shear waves.....	40
10. Conclusions.....	40
11. Summary.....	41
References.....	42

## 1. Introduction

The performance of sound absorbing materials is simulated by using proper acoustic parameters in computations. These acoustic parameters are based on the macroscopic parameters of the materials, used in the modeling. The macroscopic parameters are not mutually independent, so the efficient optimization of the materials cannot be based only on the variations of the individual macroscopic parameters. They are dependent on the microscopic parameters of the materials, the latter being more independent on each other. Also the microscopic parameters are those to which we can affect directly in manufacturing processes. The chain of the parameters is presented in Figure 1. The dependences of the parameters between different categories have to be known in order to control, e.g., what microscopic parameters have to be changed and how, to obtain good absorptive properties in selected frequency ranges.

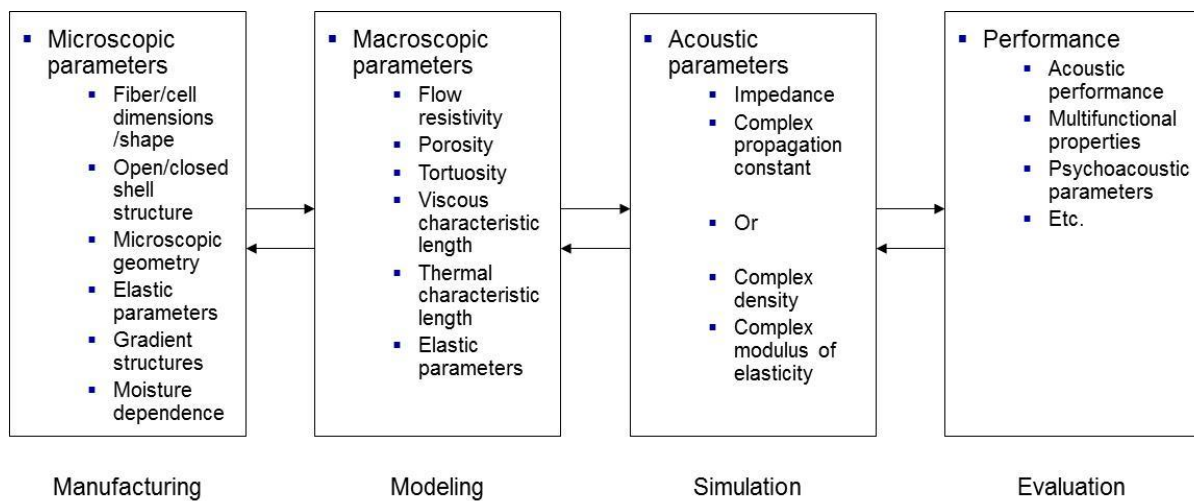


Figure 1. Chain of parameters in controlling the performance of sound absorbing materials.

In this report, the multi-scale computation method is treated for acoustical purposes, for controlling the chain of parameters in Figure 1, including the relations between the microscopic, macroscopic and acoustic parameters of sound absorbing materials. The basics of the multi-scale computation of sound absorbing materials are presented in Chapter 4, the multi-scale asymptotic method is presented in more detail in Chapter 7 and the ways of obtaining the homogenized macro-scale parameters are presented in detail in Chapter 8. Before the detailed treatment, some typical results found with multi-scale computation are presented in Chapter 5.

The dyadic notation (closely related to the tensor notation) is mostly used, to take into account possible anisotropic behaviour of materials. Most of the references assume the materials to be isotropic and scalar notation is used there. Some references take into account anisotropy by using tensor notation. Using the dyadic notation here has made it necessary to derive the equations in detail. In the literature, many writers use normalized quantities in their equations. In this report, no normalizations have been used, to get a better physical insight to the method. This also has raised the need for detailed derivations of the equations.

## 2. Goal

The goal of this study is to give a thorough presentation of the multi-scale computation method for acoustical purposes, for controlling the chain of parameters including the relations between the microscopic, macroscopic and acoustic parameters of sound absorbing materials, taking

into account possible anisotropic behaviour of materials. The second goal is to derive the relevant equations in detail, to clarify what must be assumed and at what stage to obtain the required relationships.

### 3. Models for absorptive materials

---

Absorptive materials are mostly modelled as equivalent fluids where the various acoustic properties are taken into account with complex macroscopic acoustic parameters. The simplest model for absorptive materials is the Delany-Bazley model [1], based on empirical expressions for the complex impedance and the complex wave number. Besides the fluid parameters, it only needs the flow resistivity as an input parameter. It is clear that this kind of a model is not suitable for all kinds of absorbents. Mechel [2] has done a correction to this model, for better usability at low frequencies.

The macroscopic parameters needed in the traditional models of absorbing materials are presented in Figure 2. With traditional rigid frame models, besides the fluid parameters and the flow resistivity, there are a couple of parameters that should also be known: porosity, tortuosity, viscous characteristic length and thermal characteristic length (Johnson-Champoux-Allard model). In these models, the material skeleton is assumed to be non-moving. With the limp frame model, the density of the porous material is also needed. With the Biot (elastic) model, three more parameters of the porous material are needed: Young's modulus, shear modulus (or Poisson's ratio) and loss factor, to take into account the effects of the skeleton vibration to the sound propagation. In all of these material models (despite the Delany-Bazley model and the Biot model), the complex impedance and the complex wave number are calculated through the complex density and the complex compressibility. In the Biot model, the complex density and the complex compressibility are included in the various parameters of the model in a more complicated way. The imaginary part of the density is due to the viscous losses and the imaginary part of the compressibility is due to the thermal losses of the fluid in the porous material. With these complex quantities, the basic equations of acoustics can be presented as in the fluid without any losses, the losses included in the complex parameters of the equivalent fluid. The deviations of the real parts of the density and the compressibility from their physical values take into account some other things affecting the sound propagation in the porous material, like isothermal behaviour at low frequencies and adiabatic at high frequencies (compressibility), and the fact that sound cannot propagate in rectilinear motion due to the presence of the skeleton (density).

The models treated here belong to the categories of rigid frame models and Biot model. The macro-scale complex parameters can be defined using two alternative ways: the direct numerical approach and the hybrid numerical approach. In the former, the complex parameters are directly formed from the calculated dynamic viscous and thermal permeability functions. In the latter, static viscous and thermal permeability functions, three tortuosity functions (the strict amount depending on the selection from three possible models), and the viscous and thermal characteristic lengths, are computed, from which the complex density and compressibility are finally calculated.

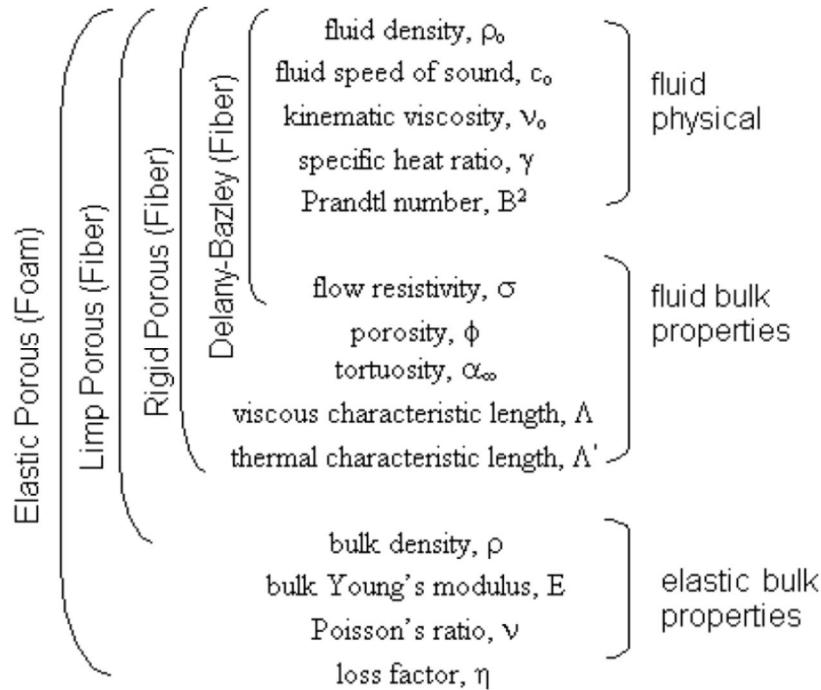


Figure 2. Macroscopic parameters of absorbents needed in the traditional models [3].

## 4. Basics of multi-scale computation of sound absorbing materials

### 4.1 Periodic structures

In setting the multi-scale equations it is supposed that the absorbing material under consideration can be handled as spatially periodic in the micro-scale, as presented in Figure 3. The material is thus assumed to include similar unit cells, Figure 4, whose volumes are  $\Omega$ . The material is said to be  $\Omega$ -periodic in the micro-scale. The fluid phase volume in each cell is  $\Omega_f$  and the fluid-solid interface surface between fibres (or foam phase) and pores in each cell is  $\Gamma$ . The solid surface  $\Gamma$  is supposed to be rigid, so no motion of the surface exists. This is the rigid-frame presumption.

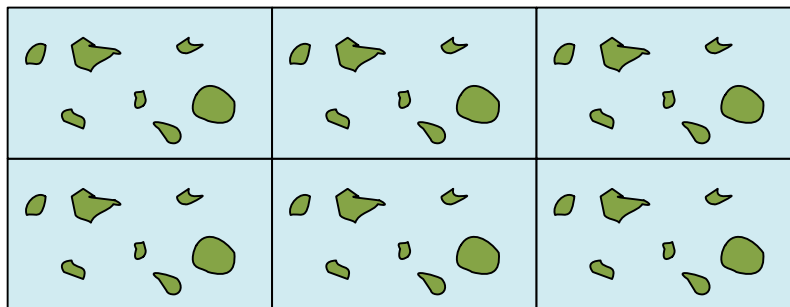


Figure 3. Periodic material.

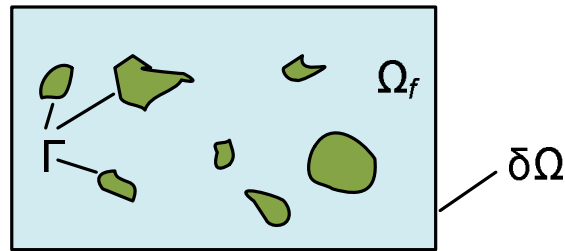


Figure 4. Unit cell of the periodic material;  $\Omega_f$  is fluid phase (pore) volume,  $\Gamma$  is interface (surface) between fibres (or foam phase) and pores; total volume of the cell is  $\Omega$  and  $\partial\Omega$  is its outer boundary.

## 4.2 Preliminaries in multi-scale computation

Before we are using the multi-scale methods, we have to specify the micro-scale geometry and microstructure features, and make some numerical model of the material in micro-scale, as presented in Figure 5. These aspects are beyond the scope of this report.

Also parameters describing the dissipation in fluid (viscosity  $\mu$ , thermal conductivity  $\kappa$ ) have to be known before using the methods.

## 4.3 Multi-scale methods

Multi-scale asymptotic method (MAM) in this context is a multi-scale approach based on an asymptotic analysis of the basic linearized equations of acoustics in the frequency domain, Eqs. (4), assuming a perfect gas with no static flow and the viscous and heat conduction effects taken into account [4, 5, 6, 7, 8]. It is used to derive a set of well-posed micro-scale equations for computing effective macro-scale variables via averaging (homogenizing) over the unit cell. So the micro-scale properties are mapped to complex macro-scale parameters of equivalent fluids via homogenization. In this approach, first two space coordinates are introduced:  $\mathbf{x}$  for the macro-variations and  $\mathbf{y}$  for the micro-variations, see Figure 9. Because of the  $\Omega$ -periodicity in the spatial coordinates (Figure 3 and Figure 4), the calculated micro-scale quantities have also to be  $\Omega$ -periodic. This is assumed throughout the following texts and it is not repeated in the following.

The structures in multi-scale methods and homogenization are presented in Figure 6. The first selection is if to use the direct numerical approach or the hybrid numerical approach [8]. In the direct approach, the equations to be solved are presented in Eq. (16) and/or (18). The direct approach requires significant computation at each frequency. Recently, an alternative and lighter, analytic-based approach has been introduced [9, 10, 11], termed as the hybrid numerical approach [8]. In this approach, there is need to solve only three static problems, static Stokes and heat conduction problems, Eq. (17) and/or (19), and electrical conduction problem, Eq. (71). According to simulations of Lee *et al.* [8], the absorption coefficient as a function of frequency, obtained from both approaches, are in very good agreement.



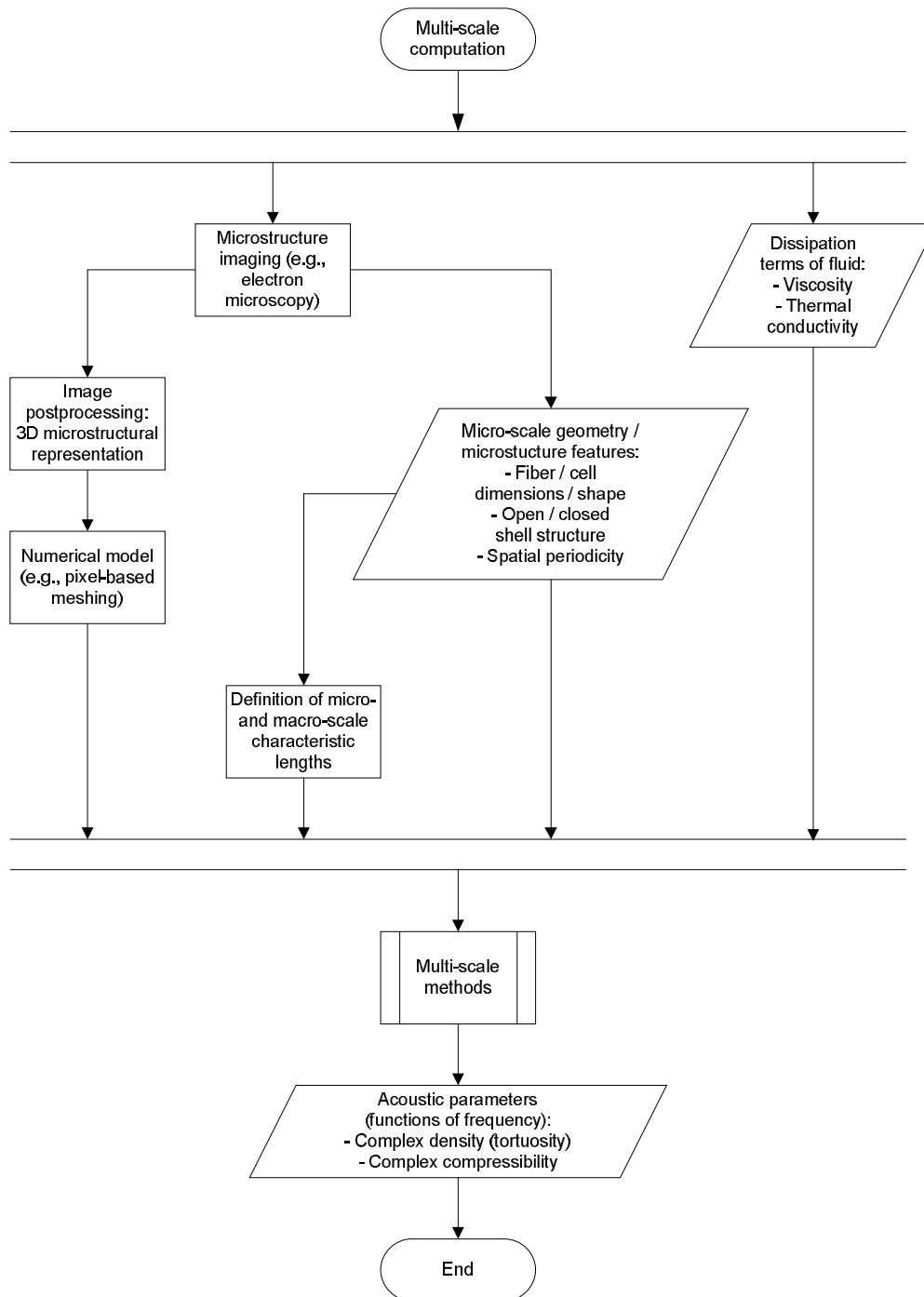


Figure 5. Flowchart of multi-scale computation of sound absorbing materials.

Multi-scale methods have been also utilized in predicting the sound absorption of multi-periodic materials like dual porosity absorbers [6] and acoustic composites [12]. The multi-period materials are not treated in this report.

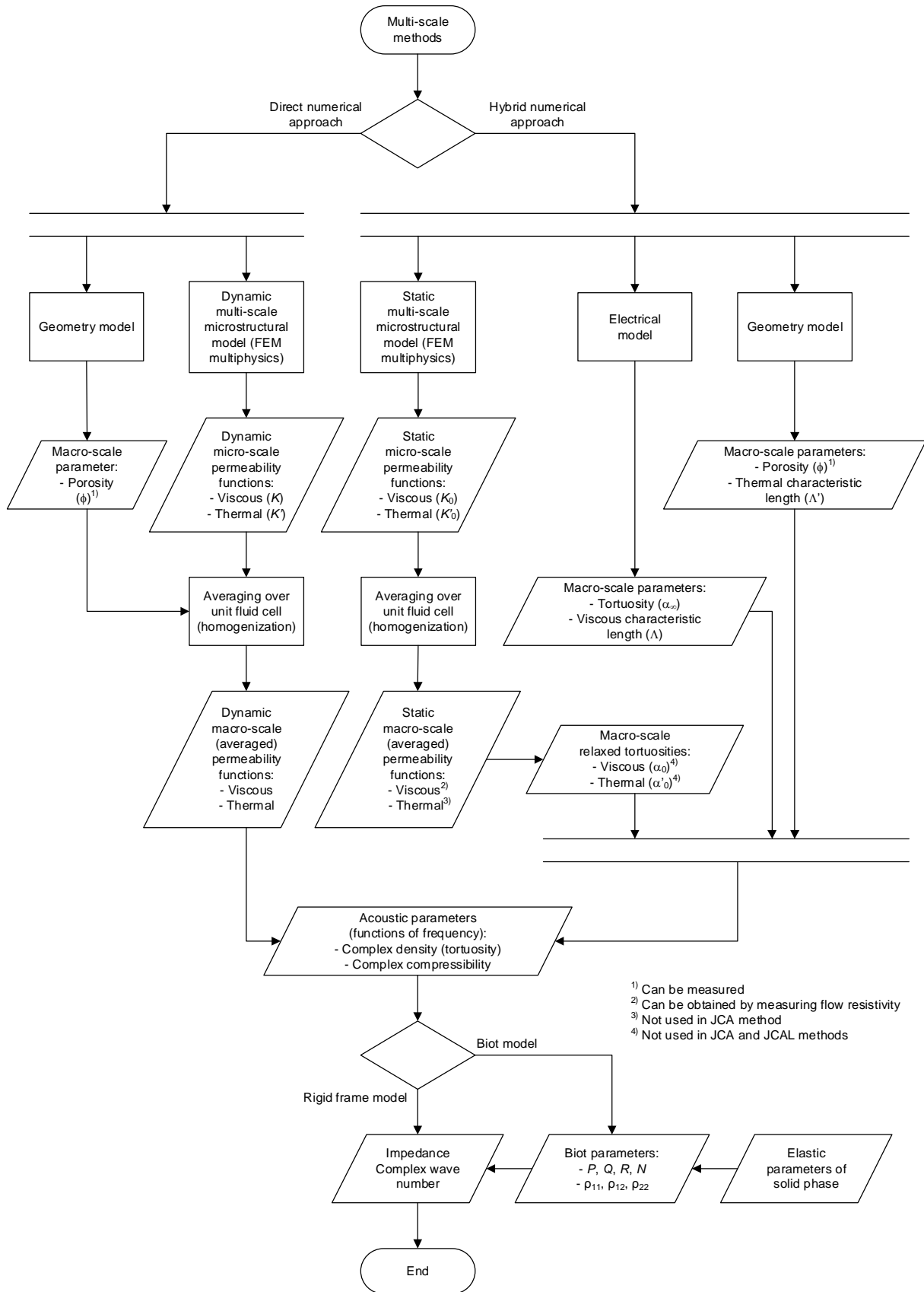


Figure 6. Flowchart of structures in multi-scale methods and homogenization in computation of sound absorbing materials.

#### 4.3.1 Direct numerical approach

In the direct numerical approach, the dynamic Stokes and dynamic heat conduction problems, Eq. (16) and/or (18), in the dynamical multi-scale microstructural model are solved to obtain the dynamic micro-scale viscous permeability function  $\vec{\mathbf{K}}(\mathbf{y}, \omega)$  and the dynamic micro-scale thermal permeability function  $K'(\mathbf{y}, \omega)$ . In the isotropic case, the viscous permeability dyadic (tensor) is replaced by scalar  $K(\mathbf{y}, \omega)$ . The corresponding macro-scale dynamic permeabilities  $\overline{\vec{\mathbf{K}}}(\omega)$  and  $\overline{K'}(\omega)$  can be obtained by homogenization (averaging over the micro-scale) according to Eq. (21). From these macro-scale permeabilities, the effective density  $\vec{\rho}_{\text{eff}}$  and its normalized version dynamic viscous tortuosity  $\vec{\alpha}(\omega)$  can be obtained using Eqs. (26) and (28) correspondingly, and the effective compressibility  $Q_{\text{eff}}$  and its normalized form  $\beta$  can be obtained using Eq. (37). Also the dynamic thermal tortuosity  $\alpha'(\omega)$ , connected to the effective compressibility, can be obtained from Eq. (38). From these parameters, the impedance, the complex sound speed and the complex wave number can be obtained using Eq. (41) with rigid frame models.

#### 4.3.2 Hybrid numerical approach

In the hybrid numerical approach, the static Stokes and heat conduction problems, Eq. (17) and/or (19), in the static multi-scale microstructural model are solved to obtain the static micro-scale viscous permeability function  $\vec{\mathbf{K}}_0(\mathbf{y}) = \vec{\mathbf{K}}(\mathbf{y}, 0)$  and the static micro-scale thermal permeability function  $K'_0(\mathbf{y}) = K'(\mathbf{y}, 0)$ . In the isotropic case, the viscous permeability dyadic (tensor) is replaced by scalar  $K_0(\mathbf{y})$ . The corresponding macro-scale static permeabilities  $\overline{\vec{\mathbf{K}}}_0$  and  $\overline{K'_0}$  can be obtained by homogenization (averaging over the micro-scale) according to Eq. (42). The permeability  $\overline{\vec{\mathbf{K}}}_0$  is related to the static flow resistivity  $\vec{\sigma}$  as stated in Eq. (45), so it also can be measured. From these macro-scale permeabilities, the viscous relaxed tortuosity  $\vec{\alpha}_0$  can be obtained from Eqs. (58), (60) or (62) (last equation for  $\alpha_0$  in isotropic case) and the thermal relaxed tortuosity  $\alpha'_0$  can be obtained from Eq. (70). The electrical conduction problem, Eq. (71), is solved to obtain the tortuosity  $\vec{\alpha}_\infty$  from Eqs. (81), (83) or (85) (last equation for  $\alpha_\infty$  in isotropic case) and the viscous characteristic length  $\vec{\Lambda}$ , according to Eqs. (107) or (106) (last equation for  $\Lambda$  in isotropic case). The thermal characteristic length  $\Lambda'$  is obtained from geometrical properties according to Eq. (112). From the parameters above, the dynamic viscous tortuosity  $\alpha(\omega)$  in the isotropic case and the normalized dynamic effective compressibility  $\beta(\omega)$  can be obtained using Eqs. (113) and (114), and the dynamic viscous tortuosity  $\vec{\alpha}(\omega)$  in the anisotropic case can be obtained using Eqs (118), (119) and (124). From these last parameters, the impedance, the complex sound speed and the complex wave number can be obtained using Eq. (41) with rigid frame models, as in the direct approach.

There are three models included in Eqs. (113) and (114) for the dynamic viscous tortuosity  $\vec{\alpha}(\omega)$  and the normalized dynamic effective compressibility. In the “Johnson-Champoux-Allard” (JCA) model, static macro-scale viscous permeability  $\overline{\vec{\mathbf{K}}}_0$  (or static flow resistivity), tortuosity  $\vec{\alpha}_\infty$ , viscous characteristic length  $\vec{\Lambda}$  and thermal characteristic length  $\Lambda'$  are used. In the “Johnson-Champoux-Allard-Lafarge” (JCAL) also static macro-scale thermal permeability  $\overline{K'_0}$  is used in addition to the former parameters. In the “Johnson-Champoux-Allard-Pride-Lafarge” (JCAPL) model also viscous and thermal relaxed tortuosities  $\vec{\alpha}_0$  and  $\alpha'_0$  are used in addition to the former parameters [13]. All models need also the porosity  $\phi$ .

### 4.3.3 Extension to Biot model

In the Biot model, the elastic behaviour of the frame is taken into account, leading to equations with three wave motions, two compressional waves and one shear wave, all of them propagating both in the air and the solid phase. The viscous and thermal effects are coupled, so the logic presented earlier for the rigid frame models cannot be directly applied. The impedance, the complex sound speed and the complex wave number cannot now be directly obtained using the effective density  $\vec{\rho}_{\text{eff}}$  or its normalized version dynamic viscous tortuosity  $\vec{\alpha}(\omega)$ , and the effective compressibility  $Q_{\text{eff}}$  or its normalized form  $\beta$  as with the rigid frame models. However, these parameters can directly be included in the parameters of the Biot model, to take into account the viscous and thermal properties of the fluid phase. These parameters, when used in the Biot parameters, can be based on either the direct numerical approach or any of the methods in the hybrid numerical approach. The internal losses of the solid phase can be taken into account in a familiar way using complex elastic parameters of the viscoelastic structure.

The Biot parameters  $P$ ,  $Q$ ,  $R$  and  $N$ , appearing in the stress-strain relationships of Eq. (125) and defined in Eqs. (127) and (128) or in (129) and (130), include, besides the bulk moduli and the shear modulus of the solid phase, also the porosity, and the effective compressibility of the fluid, the latter taking into account the thermal effects of the fluid phase. The Biot density parameters  $\vec{\rho}_{11}$ ,  $\vec{\rho}_{12}$  and  $\vec{\rho}_{22}$ , appearing in the equations of motion, Eq. (131), defined in Eq. (132), include, besides the density of the solid phase, also the porosity and the dynamic viscous tortuosity of the fluid, the latter taking into account the viscous effects of the fluid phase. The Biot equations are presented in Eq. (134), and as separated into the compressional and shear waves in Eqs. (138) and (139). The wave numbers of the compressional waves are presented in Eqs. (145) and (146) for an isotropic medium, and in Eqs. (153), (152), (147) and (154) or (155) for an anisotropic medium, and those of the shear waves for an anisotropic case in Eq. (168). The displacement relationships between the compressional waves are presented in Eqs. (157) and (158) and between the shear waves in Eqs. (164) and (165). The impedance quantities for the compressional waves are presented in Eqs. (162) and (163).

## 5. Typical results found with multi-scale computation

---

According to computations Peyrega and Jeulin [14,15], there is a frequency dependent optimum of the radii of the fibres at constant porosity for maximum sound absorption. Their explanation to that is the viscous boundary layer thickness  $\delta$ , presented in Eq. (49). Near a surface, the tangential velocity reduces exponentially to zero at the surface as a function of distance  $\xi$  to the surface, due to viscous losses of the fluid. The “range” of this phenomenon is about the boundary layer thickness, according to Figure 7. If the distance between two near-by fibres is two times the boundary layer thickness, the space between fibres is “fully occupied” by the ranges of the near-by loss regions. If the distance is smaller, all possible loss region is not used because the boundary layer thicknesses overlap, and the sound absorption is lower. With constant porosity, decreasing the radius of the fibres implies an increase of the surface area of the fibres-pore interface, thus evidently increasing the viscous losses. However, if the radius is decreased too much, the range of the loss regions of two near-by fibres overlap and the viscous losses decrease.

The viscous (and thermal) boundary layer thickness as a function of frequency is presented in Figure 8. It can be seen that the optimum radius of fibres at constant porosity is bigger at lower frequencies than at higher frequencies.

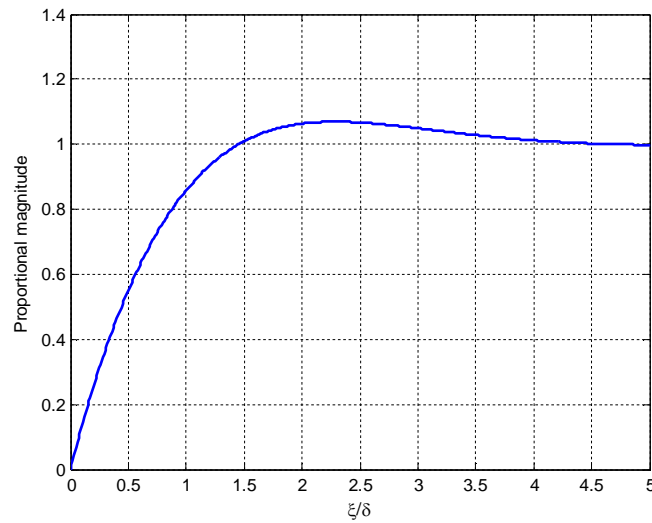


Figure 7. Proportional tangential velocity near a surface in a viscous fluid as a function of the ratio of the distance  $\xi$  to the surface and the boundary layer thickness  $\delta$ .

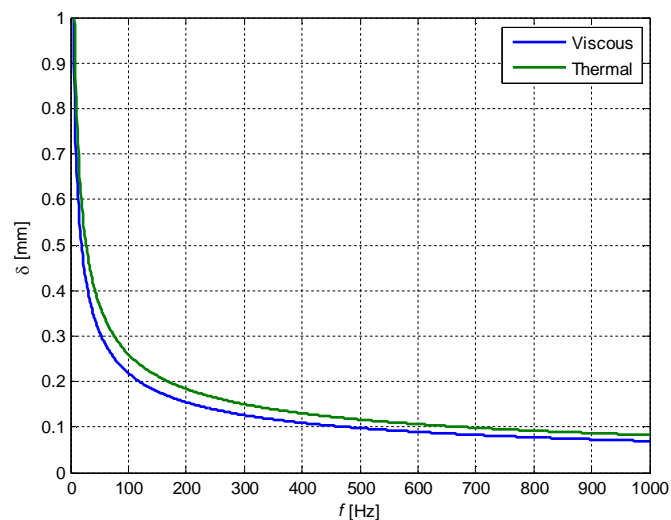


Figure 8. Viscous and thermal boundary layer thicknesses as functions of frequency [16].

According to the computations of Peyrega and Jeulin [14], for larger fibres, the absorption coefficient is globally higher for a stimulation orthogonally to the lumens than along them. Smaller fibres absorb better the acoustic energy when stimulated along their internal porosity. Absorption coefficient globally increases when the material gets thicker. However, for each radius of the fibres at each frequency, there exists a critical thickness for which the asymptotic absorption coefficient is reached, and further increasing the thickness from this does not increase the absorption coefficient. The critical thickness is the bigger and the asymptotic absorption the higher the bigger the radius of the fibre is.

According to the computations of Peyrega and Jeulin [15], randomness in unit cells in heterogeneous media gives quite similar mean absorption properties than regular cells. With bigger fibre dimensions frequency shifts are observed between the sound absorption curves of regular and random cells. In that reference, a method for determining the representative volume element of random fibrous media has been given.

According to the computations of Perrot *et al.* [11], Duval *et al.* [13], and Hoang and Perrot [17], the throat size (smallest distance between the fibres or smallest interconnecting size between opened cells of foams) and the closure rate (degree of openness inversed) of the solid films in open-cell foams play an important role in the sound absorption. Increasing the closure rate and decreasing the throat size from open-cell construction to an optimum value increases the flow resistivity and tortuosity and decreases the viscous characteristic length, improving the middle frequency performance of absorptive foams. The cell size has an effect to the selectivity of the frequency band of high sound absorption. In sound insulation applications smaller closure rates are better.

## 6. Basic field equations

The state equation of a perfect gas, the Navier-Stokes equation containing viscous effects, the equation of continuity (mass balance) and the energy balance equation containing thermal conductivity effects in a fluid domain  $\Omega_f$  without static flow can be presented in linearized formulae as (can be found in any books of acoustics, see, e.g., [18, 16])

$$\begin{aligned}
 \frac{p}{P_0} &= \frac{\rho'}{\rho_0} + \frac{T'}{T_0} \\
 \rho_0 \frac{\partial \mathbf{u}}{\partial t} &= -\nabla p + \nabla \cdot \vec{\sigma}_\mu \\
 \left( \mu_v + \frac{\mu}{3} \right) \nabla (\nabla \cdot \mathbf{u}) + \mu \nabla^2 \mathbf{u} & \\
 \frac{\partial \rho'}{\partial t} &= -\rho_0 \nabla \cdot \mathbf{u} \\
 \rho_0 c_p \frac{\partial T'}{\partial t} &= \frac{\partial p}{\partial t} + \kappa \nabla^2 T' \\
 \mathbf{u} = 0, T' = 0 & \text{ at } \Gamma,
 \end{aligned} \tag{1}$$

where  $P_0$ ,  $\rho_0$  and  $T_0$  are the static pressure, density and temperature,  $p$ ,  $\rho'$  and  $T'$  are the corresponding fluctuating (perturbation) components of the pressure, density and temperature,  $\mathbf{u}$  is the (perturbation) particle velocity,  $\kappa$  is the thermal conductivity of the fluid, and  $c_p$  is the specific heat of the fluid at constant pressure. The last line in Eqs. (1) gives the boundary conditions at the fluid-solid interface  $\Gamma$  of the fluid domain  $\Omega_f$ , the interface being supposed to obey no-slip condition for the particle velocity and isothermal condition for the perturbation temperature. The viscous stress dyadic  $\vec{\sigma}_\mu$  can be obtained from

$$\vec{\sigma}_\mu = \mu_v (\nabla \cdot \mathbf{u}) \tilde{\mathbf{I}} + \mu \left[ \nabla \mathbf{u} + (\nabla \mathbf{u})^T - \frac{2}{3} (\nabla \cdot \mathbf{u}) \tilde{\mathbf{I}} \right], \tag{2}$$

where  $\mu$  and  $\mu_v$  are the coefficient of viscosity and the expansion coefficient of viscosity of the fluid,  $\tilde{\mathbf{I}}$  is the identic dyadic, and superscript "T" means transpose. The divergence of the viscous stress dyadic in Eq. (1) is

$$\begin{aligned}
 \nabla \cdot \vec{\sigma}_\mu &= \mu_v \nabla (\nabla \cdot \mathbf{u}) + \mu \left[ \nabla^2 \mathbf{u} + \nabla (\nabla \cdot \mathbf{u}) - \frac{2}{3} \nabla (\nabla \cdot \mathbf{u}) \right] \\
 &= \left( \mu_v + \frac{\mu}{3} \right) \nabla (\nabla \cdot \mathbf{u}) + \mu \nabla^2 \mathbf{u}.
 \end{aligned} \tag{3}$$

In the frequency domain, Eqs. (1) can be presented as

$$\begin{aligned}
 \frac{p}{P_0} &= \frac{\rho'}{\rho_0} + \frac{T'}{T_0} \\
 j\omega\rho_0\mathbf{u} &= -\nabla p + \left(\mu_v + \frac{\mu}{3}\right)\nabla(\nabla\cdot\mathbf{u}) + \mu\nabla^2\mathbf{u} \\
 j\omega\rho' &= -\rho_0\nabla\cdot\mathbf{u} \\
 j\omega\rho_0c_pT' &= j\omega p + \kappa\nabla^2T' \\
 \mathbf{u} &= 0, T' = 0 \text{ at } \Gamma,
 \end{aligned}
 \tag{4}$$

where  $\omega$  is the angular frequency and  $j$  is the imaginary unit.

## 7. Multi-scale asymptotic method

In the multi-scale asymptotic method, first two space coordinates are introduced:  $\mathbf{x}$  for the macro-variations and  $\mathbf{y}$  for the micro-variations [4, 5, 6, 7, 8]

$$\mathbf{y} = \frac{\mathbf{x}}{\varepsilon}, \varepsilon = \frac{l}{L},
 \tag{5}$$

where the small parameter  $\varepsilon$  ( $\ll 1$ ) is a scale ratio of a characteristic unit cell length  $l$  and frequency dependent wavelength  $L$  according to Figure 9. For the characteristic lengths, there also exist other definitions [7, 14].

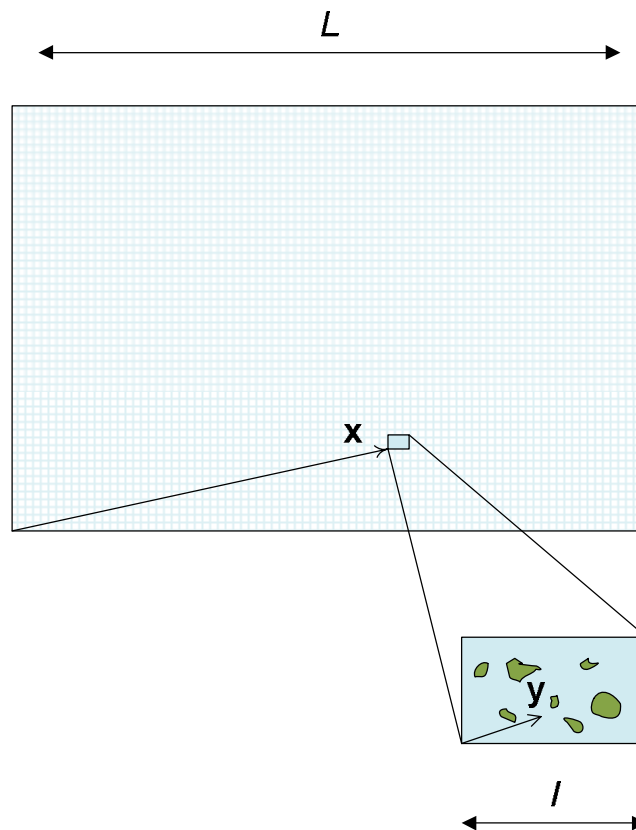


Figure 9. Characteristic lengths and macro- and micro-variation coordinates in periodic materials.

## 7.1 Power series in multi-scale method

The desired solution variables are split into their macroscopic and microscopic components by using power series involving  $\varepsilon$  as [4, 5, 6, 7, 8]

$$\begin{aligned}\mathbf{u} &= \mathbf{u}_0(\mathbf{x}, \mathbf{y}) + \varepsilon \mathbf{u}_1(\mathbf{x}, \mathbf{y}) + \varepsilon^2 \mathbf{u}_2(\mathbf{x}, \mathbf{y}) + \dots \\ p &= p_0(\mathbf{x}, \mathbf{y}) + \varepsilon p_1(\mathbf{x}, \mathbf{y}) + \varepsilon^2 p_2(\mathbf{x}, \mathbf{y}) + \dots \\ T' &= T'_0(\mathbf{x}, \mathbf{y}) + \varepsilon T'_1(\mathbf{x}, \mathbf{y}) + \varepsilon^2 T'_2(\mathbf{x}, \mathbf{y}) + \dots\end{aligned}\quad (6)$$

Because variables  $\mathbf{x}$  and  $\mathbf{y}$  are dependent, we obtain [5]

$$\frac{d}{dx_i} = \frac{\partial}{\partial x_i} + \frac{\partial y_i}{\partial x_i} \frac{\partial}{\partial y_i} = \frac{\partial}{\partial x_i} + \frac{1}{\varepsilon} \frac{\partial}{\partial y_i}, \quad (7)$$

and the differential operators gradient and Laplacian take the form

$$\begin{aligned}\nabla &= \nabla_x + \frac{1}{\varepsilon} \nabla_y \\ \nabla^2 &= \nabla_x^2 + \frac{2}{\varepsilon} \nabla_{xy}^2 + \frac{1}{\varepsilon^2} \nabla_y^2.\end{aligned}\quad (8)$$

## 7.2 Power series of basic field equations

Inserting the differential operators above to Eqs. (4) we obtain

$$\begin{aligned}\frac{p}{P_0} &= \frac{\rho'}{\rho_0} + \frac{T'}{T_0} \\ j\omega \rho_0 \mathbf{u} &= -\left(\nabla_x + \frac{1}{\varepsilon} \nabla_y\right) p + \left(\mu_v + \frac{\mu}{3}\right) \left(\nabla_x + \frac{1}{\varepsilon} \nabla_y\right) \left[\left(\nabla_x + \frac{1}{\varepsilon} \nabla_y\right) \cdot \mathbf{u}\right] + \\ &\quad + \mu \left(\nabla_x^2 + \frac{2}{\varepsilon} \nabla_{xy}^2 + \frac{1}{\varepsilon^2} \nabla_y^2\right) \mathbf{u} \\ j\omega \frac{\rho'}{\rho_0} &= -\left(\nabla_x + \frac{1}{\varepsilon} \nabla_y\right) \cdot \mathbf{u} \\ j\omega \rho_0 c_p T' &= j\omega p + \kappa \left(\nabla_x^2 + \frac{2}{\varepsilon} \nabla_{xy}^2 + \frac{1}{\varepsilon^2} \nabla_y^2\right) T' \\ \mathbf{u} &= 0, T' = 0 \text{ at } \Gamma.\end{aligned}\quad (9)$$

Inserting the first equation above to the third one and making some rearrangements we obtain further



$$\begin{aligned}
 j\omega\rho_0\mathbf{u} &= -\nabla_x p - \frac{1}{\varepsilon}\nabla_y p + \left(\mu_v + \frac{\mu}{3}\right)\left[\left(\nabla_x\nabla_x \cdot \mathbf{u} + \frac{1}{\varepsilon}\nabla_x\nabla_y \cdot \mathbf{u}\right)\right] + \\
 &+ \left(\mu_v + \frac{\mu}{3}\right)\left[\left(\frac{1}{\varepsilon}\nabla_y\nabla_x \cdot \mathbf{u} + \frac{1}{\varepsilon^2}\nabla_y\nabla_y \cdot \mathbf{u}\right)\right] + \mu\nabla_x^2\mathbf{u} + \frac{2}{\varepsilon}\mu\nabla_{xy}^2\mathbf{u} + \frac{1}{\varepsilon^2}\mu\nabla_y^2\mathbf{u} \\
 j\omega\left(\frac{p}{P_0} - \frac{T'}{T_0}\right) &= -\nabla_x \cdot \mathbf{u} - \frac{1}{\varepsilon}\nabla_y \cdot \mathbf{u} \\
 j\omega\rho_0 c_p T' &= j\omega p + \kappa\nabla_x^2 T' + \frac{2}{\varepsilon}\kappa\nabla_{xy}^2 T' + \frac{1}{\varepsilon^2}\kappa\nabla_y^2 T' \\
 \mathbf{u} = 0, T' = 0 &\text{ at } \Gamma.
 \end{aligned} \tag{10}$$

The viscosity and thermal conductivity terms are of the order  $\varepsilon^2$  compared to other terms [6], so this can be taken into account by marking [5]

$$\begin{aligned}
 \mu &= \varepsilon^2 \mu' \\
 \mu_v &= \varepsilon^2 \mu'_v \\
 \kappa &= \varepsilon^2 \kappa'.
 \end{aligned} \tag{11}$$

Inserting the power series (6) and Eq. (11) into presentation (10) and taking a few first terms into account we obtain

$$\begin{aligned}
 j\omega\rho_0\mathbf{u}_0 &= -\nabla_x p_0 - \frac{1}{\varepsilon}\nabla_y p_0 - \nabla_y p_1 + \varepsilon^2\left(\mu'_v + \frac{\mu'}{3}\right)\left[\left(\frac{1}{\varepsilon^2}\nabla_y\nabla_y \cdot \mathbf{u}_0\right)\right] + \varepsilon^2\mu' \frac{1}{\varepsilon^2}\nabla_y^2\mathbf{u}_0 \\
 j\omega\left(\frac{p_0}{P_0} - \frac{T'_0}{T_0}\right) &= -\nabla_x \cdot \mathbf{u}_0 - \frac{1}{\varepsilon}\nabla_y \cdot \mathbf{u}_0 - \nabla_y \cdot \mathbf{u}_1 \\
 j\omega\rho_0 c_p T'_0 &= j\omega p_0 + \varepsilon^2\kappa' \frac{1}{\varepsilon^2}\nabla_y^2 T'_0 \\
 \mathbf{u}_0 = 0, \mathbf{u}_1 = 0, T'_0 = 0 &\text{ at } \Gamma.
 \end{aligned} \tag{12}$$

### 7.3 Equations of multi-scale method for sound absorbing materials

Separating the two highest orders ( $\varepsilon^{-1}$  and  $\varepsilon^0$ ) from the two first equations in Eqs. (12) and the highest order ( $\varepsilon^0$ ) from the third equation we obtain further

$$\begin{aligned}
 \nabla_y p_0 &= 0 \\
 j\omega\rho_0\mathbf{u}_0 &= -\nabla_x p_0(\mathbf{x}) - \nabla_y p_1 + \mu'\nabla_y^2\mathbf{u}_0 \\
 \nabla_y \cdot \mathbf{u}_0 &= 0 \\
 j\omega\left(\frac{p_0(\mathbf{x})}{P_0} - \frac{T'_0}{T_0}\right) &= -\nabla_x \cdot \mathbf{u}_0 - \nabla_y \cdot \mathbf{u}_1 \\
 j\omega\rho_0 c_p T'_0 &= j\omega p_0(\mathbf{x}) + \kappa'\nabla_y^2 T'_0 \\
 \mathbf{u}_0 = 0, \mathbf{u}_1 = 0, T'_0 = 0 &\text{ at } \Gamma.
 \end{aligned} \tag{13}$$

So  $p_0$  is only function of  $\mathbf{x}$  and the divergence of  $\mathbf{u}_0$  in the micro-scale vanishes, and the equations above may be written as

$$\begin{aligned}
 j\omega\rho_0\mathbf{u}_0 - \mu'\nabla_y^2\mathbf{u}_0 + \nabla_y p_1 &= -\nabla_x p_0(\mathbf{x}) \\
 j\omega\frac{P_0}{T_0}T'_0 - P_0\nabla_x \cdot \mathbf{u}_0 - P_0\nabla_y \cdot \mathbf{u}_1 &= j\omega p_0(\mathbf{x}) \\
 j\omega\rho_0 c_p T'_0 - \kappa'\nabla_y^2 T'_0 &= j\omega p_0(\mathbf{x}) \\
 \nabla_y \cdot \mathbf{u}_0 &= 0 \\
 \mathbf{u}_0 = 0, \mathbf{u}_1 = 0, T'_0 &= 0 \text{ at } \Gamma.
 \end{aligned} \tag{14}$$

It is assumed that  $T'_0$ ,  $p_1$  and  $\mathbf{u}_0$  can be obtained by using a scalar operator  $K'$ , a vector operator  $\mathbf{\Pi}$  and a dyadic (or tensor) operator  $\vec{\mathbf{K}}$  from following presentations [7]

$$\begin{aligned}
 T'_0 &= \frac{1}{\kappa} K'(\mathbf{y}, \omega) [j\omega p_0(\mathbf{x})] \\
 p_1 &= \mathbf{\Pi}(\mathbf{y}, \omega) \cdot [-\nabla_x p_0(\mathbf{x})] \\
 \mathbf{u}_0 &= \frac{1}{\mu} \vec{\mathbf{K}}(\mathbf{y}, \omega) \cdot [-\nabla_x p_0(\mathbf{x})]
 \end{aligned} \tag{15}$$

The last equation in (15) is the dynamic Darcy's law in the micro-scale [15] and the first equation is its thermal analogy.

Inserting these into Eq. (14), reducing common factors from them, re-using Eq. (11), and substituting  $(1/\varepsilon)\nabla_y$  with  $\nabla$  according to Eq. (8) (noticing that the variables are not functions of macro-variation coordinates  $x$ ), we obtain equations for the three operators [7]

$$\begin{aligned}
 \frac{j\omega\rho_0}{\mu} \vec{\mathbf{K}} - \nabla^2 \vec{\mathbf{K}} + \nabla \mathbf{\Pi} &= \vec{\mathbf{I}} \\
 \frac{j\omega\rho_0 c_p}{\kappa} K' - \nabla^2 K' &= 1 \\
 \nabla \cdot \vec{\mathbf{K}} &= 0 \\
 \vec{\mathbf{K}} = 0, K' = 0 &\text{ at } \Gamma.
 \end{aligned} \tag{16}$$

The first equation in (16) is the dynamic (unsteady) Stokes problem and the second one the dynamic heat conduction problem.

At zero frequency Eq. (16) leads to

$$\begin{aligned}
 -\nabla^2 \vec{\mathbf{K}} + \nabla \mathbf{\Pi} &= \vec{\mathbf{I}} \\
 -\nabla^2 K' &= 1 \\
 \nabla \cdot \vec{\mathbf{K}} &= 0 \\
 \vec{\mathbf{K}} = 0, K' = 0 &\text{ at } \Gamma.
 \end{aligned} \tag{17}$$

The first equation in (17) is the static (steady) Stokes problem and the second one the static heat conduction problem.

For calculating purposes, the Stokes problem can be further developed into a vector form by multiplying it with a unit vector  $\mathbf{e}_i$ . For the dynamic Stokes problem we obtain

$$\begin{aligned}
 \frac{j\omega\rho_0}{\mu}(\vec{\mathbf{K}} \cdot \mathbf{e}_i) - \nabla^2(\vec{\mathbf{K}} \cdot \mathbf{e}_i) + \nabla(\mathbf{\Pi} \cdot \mathbf{e}_i) &= \mathbf{e}_i \\
 \nabla \cdot (\vec{\mathbf{K}} \cdot \mathbf{e}_i) &= 0 \\
 \vec{\mathbf{K}} \cdot \mathbf{e}_i &= 0 \text{ at } \Gamma
 \end{aligned} \tag{18}$$

and for the static Stokes problem

$$\begin{aligned}
 -\nabla^2(\vec{\mathbf{K}} \cdot \mathbf{e}_i) + \nabla(\mathbf{\Pi} \cdot \mathbf{e}_i) &= \mathbf{e}_i \\
 \nabla \cdot (\vec{\mathbf{K}} \cdot \mathbf{e}_i) &= 0 \\
 \vec{\mathbf{K}} \cdot \mathbf{e}_i &= 0 \text{ at } \Gamma.
 \end{aligned} \tag{19}$$

These equations can be solved for three orthogonal unit vectors  $\mathbf{e}_i$ , to obtain the dyadic  $\vec{\mathbf{K}}$ . With the formulae above, it has been utilized that the identic dyadic can be presented as

$$\vec{\mathbf{I}} = \mathbf{e}_{y1}\mathbf{e}_{y1} + \mathbf{e}_{y2}\mathbf{e}_{y2} + \mathbf{e}_{y3}\mathbf{e}_{y3}. \tag{20}$$

It should be noted that Eqs. (18) and (19) need a constraint for  $\mathbf{\Pi} \cdot \mathbf{e}_i$  at some point. Without that the equations cannot be solved with FEM programs.<sup>1</sup>

## 8. Homogenized macro-scale parameters

### 8.1 Direct numerical approach

Solving Eqs. (16) and/or (18), we obtain terms  $\vec{\mathbf{K}}(\mathbf{y}, \omega)$  and  $K'(\mathbf{y}, \omega)$ . The first is the micro-scale dynamic viscous permeability function and the latter is the micro-scale dynamic thermal permeability function.

The macro-scale dynamic permeabilities can be obtained by homogenization (averaging over the micro-scale) [7, 10]

$$\begin{aligned}
 \overline{\vec{\mathbf{K}}}(\omega) &= \phi \langle \vec{\mathbf{K}}(\mathbf{y}, \omega) \rangle_{\mathbf{y}} \\
 \overline{K'}(\omega) &= \phi \langle K'(\mathbf{y}, \omega) \rangle_{\mathbf{y}},
 \end{aligned} \tag{21}$$

where the average  $\langle \cdot \rangle_{\mathbf{y}}$  is taken in the fluid domain  $\Omega_f$  of a cell. The macro-scale dynamic viscous permeability  $\overline{\vec{\mathbf{K}}}(\omega)$  is a symmetric dyadic [5].

The porosity  $\phi$  needed above can be defined as

$$\phi = \frac{\int_{\Omega_f} d\Omega}{\int_{\Omega} d\Omega} = \frac{\Omega_f}{\Omega}, \tag{22}$$

<sup>1</sup> Private communication with Comsol Oy.

so it is the ratio of fluid phase volume to the total volume of a cell.

The last and first equation in (15) can be presented macro-scale as

$$\begin{aligned}\phi\langle\mathbf{u}_0\rangle_y &= -\frac{1}{\mu}\overline{\overline{\mathbf{K}}}(\omega)\cdot\nabla_x p_0(\mathbf{x}) \\ \phi\langle T'_0\rangle_y &= \frac{1}{\kappa}\overline{\overline{K'}}(\omega)[j\omega p_0(\mathbf{x})].\end{aligned}\quad (23)$$

### 8.1.1 Effective density

From the first equation of (23) we can obtain

$$\nabla_x p_0(\mathbf{x}) = -\mu\phi\overline{\overline{\mathbf{K}}}(\omega)^{-1}\cdot\langle\mathbf{u}_0\rangle_y, \quad (24)$$

where superscript “-1” means inverse of a dyadic.

Comparing this to the second equation of (4), with the viscous effects included to the “effective density” dyadic (tensor)  $\overrightarrow{\overrightarrow{\rho}}_{\text{eff}}$  in the macro-scale

$$\nabla_x p_0(\mathbf{x}) = -j\omega\overrightarrow{\overrightarrow{\rho}}_{\text{eff}}\cdot\langle\mathbf{u}_0\rangle_y, \quad (25)$$

we can see that the effective density can be obtained from [8, 15]

$$\overrightarrow{\overrightarrow{\rho}}_{\text{eff}} = \frac{\mu\phi}{j\omega}\overline{\overline{\mathbf{K}}}(\omega)^{-1}. \quad (26)$$

### 8.1.2 Dynamic viscous tortuosity

The dynamic viscous tortuosity dyadic (or tensor)  $\overrightarrow{\overrightarrow{\alpha}}$  can be defined via [19, 7, 10]

$$\nabla_x p_0(\mathbf{x}) = -j\omega\rho_0\overrightarrow{\overrightarrow{\alpha}}(\omega)\cdot\langle\mathbf{u}_0\rangle_y. \quad (27)$$

Comparing this to Eqs. (24) and (25) we obtain

$$\overrightarrow{\overrightarrow{\alpha}}(\omega) = \frac{\overrightarrow{\overrightarrow{\rho}}_{\text{eff}}}{\rho_0} = \frac{\mu\phi}{j\omega\rho_0}\overline{\overline{\mathbf{K}}}(\omega)^{-1}. \quad (28)$$

It can be seen that the dynamic viscous tortuosity is the same as the normalized effective density.

Because the macro-scale dynamic viscous permeability is a symmetric dyadic, the dynamic viscous tortuosity and the effective density also are symmetric dyadics.

### 8.1.3 Effective compressibility

The second equation in (14) is in macro-scale

$$j\omega\frac{P_0}{T_0}\langle T'_0\rangle_y - P_0\langle\nabla_x\cdot\mathbf{u}_0\rangle_y - P_0\langle\nabla_y\cdot\mathbf{u}_1\rangle_y = j\omega p_0(\mathbf{x}). \quad (29)$$

Using Gauss theorem it can be seen that

$$\langle \nabla_y \cdot \mathbf{u}_1 \rangle_y = \frac{1}{\Omega_f} \int_{\Omega_f} \nabla_y \cdot \mathbf{u}_1 \, d\Omega = \frac{1}{\Omega_f} \oint_{\Gamma+\partial\Omega} \mathbf{u}_1 \cdot \mathbf{e}_n \, dS = 0, \quad (30)$$

where  $\mathbf{e}_n$  is the unit normal vector on the boundary surfaces. The surface integral vanishes at  $\Gamma$ , due to the boundary conditions in Eq. (14). It vanishes also at  $\partial\Omega$ , due to  $\Omega$ -periodicity of the fields.

Using the result of Eq. (30) and applying the second equation of (23), we obtain from Eq. (29)

$$j\omega \frac{P_0}{T_0} \frac{1}{\kappa} \langle K'(\mathbf{y}, \omega) \rangle_y j\omega p_0(\mathbf{x}) - P_0 \langle \nabla_x \cdot \mathbf{u}_0 \rangle_y = j\omega p_0(\mathbf{x}), \quad (31)$$

from which we can further obtain

$$\begin{aligned} \langle \nabla_x \cdot \mathbf{u}_0 \rangle_y &= -\frac{1}{P_0} j\omega p_0(\mathbf{x}) \left( 1 - j\omega \frac{P_0}{\kappa T_0} \langle K'(\mathbf{y}, \omega) \rangle_y \right) \\ &= -\frac{1}{\gamma P_0} j\omega p_0(\mathbf{x}) \left( \gamma - j\omega(\gamma - 1) \frac{P_0 c_P}{\kappa \phi} \overline{K'(\omega)} \right), \end{aligned} \quad (32)$$

where the state equation for a perfect gas has been utilized in the form

$$\frac{P_0}{\rho_0 T_0} = R = \frac{(\gamma - 1)c_P}{\gamma}, \quad (33)$$

where  $R$  is the gas constant and  $\gamma$  is the adiabatic constant.

Without thermal losses the third equation of (4) in the macro-scale can be presented as

$$\langle \nabla_x \cdot \mathbf{u}_0 \rangle_y = -j\omega Q_0 p_0(\mathbf{x}), \quad (34)$$

where the compressibility  $Q_0$  is

$$Q_0 = \frac{1}{\gamma P_0}. \quad (35)$$

Comparing Eq. (32) to Eq. (34), with the thermal effects included to the “effective compressibility”  $Q_{\text{eff}}$  in the macro-scale (without thermal losses)

$$\langle \nabla_x \cdot \mathbf{u}_0 \rangle_y = -j\omega Q_{\text{eff}} p_0(\mathbf{x}), \quad (36)$$

we can see that the effective compressibility can be obtained from [7, 8, 15]

$$\begin{aligned} Q_{\text{eff}} &= Q_0 \beta \\ \beta &= \gamma - j\omega(\gamma - 1) \frac{P_0 c_P}{\kappa \phi} \overline{K'(\omega)}. \end{aligned} \quad (37)$$

$$Q_0 = \frac{1}{\gamma P_0},$$

where  $\beta$  is the normalized effective compressibility.

#### 8.1.4 Dynamic thermal tortuosity

The dynamic thermal tortuosity can be defined analogously with the viscous one, Eq. (28) (latter formula), as

$$\alpha'(\omega) = \frac{\kappa\phi}{j\omega\rho_0 c_p} \overline{K}'(\omega)^{-1}. \quad (38)$$

Using this definition, the second equation in (23) can be presented as

$$p_0(\mathbf{x}) = \rho_0 c_p \alpha'(\omega) \langle T_0' \rangle_y. \quad (39)$$

Comparing Eqs. (37) and (38), the normalized effective compressibility can be written as

$$\beta = \gamma - \frac{\gamma - 1}{\alpha'(\omega)}. \quad (40)$$

#### 8.1.5 Effective sound speed and characteristic impedance in rigid frame models

The effective characteristic impedance  $Z$ , the effective complex sound speed  $c_{\text{eff}}$  [15] and the complex wave number  $\mathbf{k}$  of the homogenized porous medium can now be obtained from the effective complex density (or tortuosity) and compressibility from the following formulae

$$\begin{aligned} Z &= \frac{1}{\phi} \sqrt{\frac{\mathbf{e}_1 \cdot \vec{\rho}_{\text{eff}} \cdot \mathbf{e}_1}{Q_{\text{eff}}}} = \frac{\rho_0 c_0}{\phi} \sqrt{\frac{\mathbf{e}_1 \cdot \vec{\alpha}(\omega) \cdot \mathbf{e}_1}{\beta(\omega)}} \\ c_{\text{eff}} &= \sqrt{\frac{\mathbf{e}_1 \cdot \vec{\rho}_{\text{eff}}^{-1} \cdot \mathbf{e}_1}{Q_{\text{eff}}}} = c_0 \sqrt{\frac{\mathbf{e}_1 \cdot \vec{\alpha}(\omega)^{-1} \cdot \mathbf{e}_1}{\beta(\omega)}} \\ \mathbf{k} &= k \mathbf{e}_1 = \frac{\omega}{c_{\text{eff}}} \mathbf{e}_1, \end{aligned} \quad (41)$$

where  $\mathbf{e}_1$  is the unit vector in the propagation direction of the acoustic wave and  $c_0$  is the speed of sound in free space. These equations hold for rigid frame models.

## 8.2 Hybrid numerical approach

The direct approach requires significant computation at each frequency. In the hybrid numerical approach, there is need to solve only three static problems, static Stokes problem (first equation in (17) or Eq. (19)), static heat conduction problem (second equation in (17)) and electrical conduction problem (presented later, Eq. (71)).

Solving Eqs. (17) and/or (19) we obtain static permeabilities  $\vec{\mathbf{K}}_0(\mathbf{y}) = \vec{\mathbf{K}}(\mathbf{y}, 0)$  and  $K_0(\mathbf{y}) = K(\mathbf{y}, 0)$ . The first is the micro-scale static viscous permeability function and the latter is the micro-scale static thermal permeability function.

The macro-scale static permeabilities can be obtained by homogenization (averaging over the micro-scale) [10, 9, 11]

$$\begin{aligned} \vec{\mathbf{K}}_0 &= \phi \langle \vec{\mathbf{K}}_0(\mathbf{y}) \rangle_y \\ K_0 &= \phi \langle K_0(\mathbf{y}) \rangle_y, \end{aligned} \quad (42)$$

At low frequencies, the first equation in (23) can be written as

$$\phi\langle \mathbf{u}_0 \rangle_y = -\frac{1}{\mu} \overline{\overline{\mathbf{K}}_0} \cdot \nabla_x p_0(\mathbf{x}). \quad (43)$$

The macroscopic definition of the static flow resistivity  $\overleftrightarrow{\sigma}$  can be presented as

$$\phi\langle \mathbf{u}_0 \rangle_y = -\overleftrightarrow{\sigma}^{-1} \cdot \nabla_x p_0(\mathbf{x}). \quad (44)$$

Comparing Eqs. (43) and (44), we can see that [20]

$$\overline{\overline{\mathbf{K}}_0} = \mu \overleftrightarrow{\sigma}^{-1}. \quad (45)$$

The dynamic viscous and thermal tortuosities at low frequencies can be written, using Eqs. (28) and (38), approximately as

$$\begin{aligned} \lim\{\overleftrightarrow{\alpha}(\omega)\} &= \frac{\mu\phi}{j\omega\rho_0} \overline{\overline{\mathbf{K}}_0}^{-1} + \overleftrightarrow{\alpha}_0, \omega \rightarrow 0 \\ \lim\{\alpha'(\omega)\} &= \frac{\kappa\phi}{j\omega\rho_0 c_p} \overline{\overline{K}'_0}^{-1} + \alpha'_0, \omega \rightarrow 0, \end{aligned} \quad (46)$$

where  $\overleftrightarrow{\alpha}_0$  and  $\alpha'_0$  are the viscous and thermal "relaxed" tortuosities, appearing as the first (real-valued constant) corrections to the leading imaginary terms having  $(j\omega)^{-1}$  [9].

The viscous and thermal tortuosities at infinite frequencies are defined by

$$\begin{aligned} \overleftrightarrow{\alpha}_\infty &= \overleftrightarrow{\alpha}(\infty) \\ \alpha'_\infty &= \alpha'(\infty). \end{aligned} \quad (47)$$

The viscous and thermal characteristic lengths  $\Lambda$  and  $\Lambda'$  are defined by limiting values of  $\alpha$  and  $\langle T'_0 \rangle$  when the frequency is high [19, 20]

$$\begin{aligned} \lim\{\alpha(\omega)\} &= \alpha_\infty \left[ 1 + (1-j) \frac{\delta}{\Lambda} \right], \quad \omega \rightarrow \infty \\ \lim\{\langle T'_0 \rangle\} &= T'_{00} \left[ 1 - (1-j) \frac{\delta'}{\Lambda'} \right], \quad \omega \rightarrow \infty, \end{aligned} \quad (48)$$

where  $T'_{00}$  is the temperature without thermal boundary losses, and  $\delta$  and  $\delta'$  are the viscous and thermal boundary layer thicknesses

$$\begin{aligned} \delta &= \sqrt{\frac{2\mu}{\omega\rho_0}} \\ \delta' &= \sqrt{\frac{2\kappa}{\omega\rho_0 c_p}}. \end{aligned} \quad (49)$$

These limiting values of tortuosities and the characteristic lengths are treated in the following.

8.2.1 Viscous relaxed tortuosity  $\alpha_0$ 

Multiplying the first equation of (14) by  $\mathbf{u}_0^*$  (\* meaning complex conjugate) and averaging this equation over the fluid domain, we obtain (the corresponding boundary condition and zero divergence condition included)

$$\begin{aligned} j\omega\rho_0 \langle \mathbf{u}_0 \cdot \mathbf{u}_0^* \rangle_y - \mu' \langle (\nabla_y^2 \mathbf{u}_0) \cdot \mathbf{u}_0^* \rangle_y + \langle (\nabla_y p_1) \cdot \mathbf{u}_0^* \rangle_y &= -\nabla_x p_0(\mathbf{x}) \cdot \langle \mathbf{u}_0^* \rangle_y \\ \nabla_y \cdot \mathbf{u}_0 &= 0 \quad \nabla_y \cdot \mathbf{u}_0^* = 0 \\ \mathbf{u}_0 &= 0, \mathbf{u}_0^* = 0 \text{ at } \Gamma. \end{aligned} \quad (50)$$

Integrating by parts, using Gauss theorem, and utilizing the third line in Eq. (50), the averaged part of the second term in Eq. (50) can be presented as

$$\begin{aligned} \langle (\nabla_y^2 \mathbf{u}_0) \cdot \mathbf{u}_0^* \rangle_y &= -\langle (\nabla_y \times \nabla_y \times \mathbf{u}_0) \cdot \mathbf{u}_0^* \rangle_y = \\ &= -\langle \nabla_y \cdot [(\nabla_y \times \mathbf{u}_0) \times \mathbf{u}_0^*] \rangle_y - \langle (\nabla_y \times \mathbf{u}_0) \cdot (\nabla_y \times \mathbf{u}_0^*) \rangle_y = \\ &= -\frac{1}{\Omega_f} \oint_{\Gamma+\partial\Omega} [(\nabla_y \times \mathbf{u}_0) \times \mathbf{u}_0^*] \cdot \mathbf{e}_n \, dS - \langle (\nabla_y \times \mathbf{u}_0) \cdot (\nabla_y \times \mathbf{u}_0^*) \rangle_y = \\ &= -\langle (\nabla_y \times \mathbf{u}_0) \cdot (\nabla_y \times \mathbf{u}_0^*) \rangle_y. \end{aligned} \quad (51)$$

The surface integral vanishes at  $\Gamma$ , due to the boundary conditions in Eq. (50). It vanishes also at  $\partial\Omega$ , due to  $\Omega$ -periodicity of the fields.

Integrating by parts, using Gauss theorem, and utilizing the second and third lines in Eq. (50), the third term in the equation above can be seen to vanish

$$\begin{aligned} \langle (\nabla_y p_1) \cdot \mathbf{u}_0^* \rangle_y &= -\langle p_1 \nabla_y \cdot \mathbf{u}_0^* \rangle_y + \langle \nabla_y \cdot (p_1 \mathbf{u}_0^*) \rangle_y = \\ \langle \nabla_y \cdot (p_1 \mathbf{u}_0^*) \rangle_y &= \frac{1}{\Omega_f} \oint_{\Gamma+\partial\Omega} p_1 \mathbf{u}_0^* \cdot \mathbf{e}_n \, dS = 0. \end{aligned} \quad (52)$$

Also now, the surface integral vanishes at  $\Gamma$ , due to the boundary conditions in Eq. (50), and at  $\partial\Omega$ , due to  $\Omega$ -periodicity of the fields.

The definition of the dynamic viscous tortuosity, Eq. (27), can be presented at low frequencies, according to the first equation in (46), as

$$\nabla_x p_0(\mathbf{x}) = -j\omega\rho_0 \left( \frac{\mu\phi}{j\omega\rho_0} \overline{\overline{\mathbf{K}_0}}^{-1} + \vec{\alpha}_0 \right) \cdot \langle \mathbf{u}_0 \rangle_y = -\left( \mu\phi \overline{\overline{\mathbf{K}_0}}^{-1} + j\omega\rho_0 \vec{\alpha}_0 \right) \cdot \langle \mathbf{u}_0 \rangle_y. \quad (53)$$

Now Eq. (50) can be presented, using Eqs. (51), (52) and (53) as

$$j\omega\rho_0 \langle \mathbf{u}_0 \cdot \mathbf{u}_0^* \rangle_y + \mu' \langle (\nabla_y \times \mathbf{u}_0) \cdot (\nabla_y \times \mathbf{u}_0^*) \rangle_y = \left( \mu\phi \overline{\overline{\mathbf{K}_0}}^{-1} + j\omega\rho_0 \vec{\alpha}_0 \right) \cdot \langle \mathbf{u}_0 \rangle_y \cdot \langle \mathbf{u}_0^* \rangle_y. \quad (54)$$

The macro-scale static permeabilities and the relaxed tortuosities are real valued. Making the imaginary parts to match in Eq. (54), we obtain

$$\langle \mathbf{u}_0 \cdot \mathbf{u}_0^* \rangle_y = \langle \mathbf{u}_0^* \rangle_y \cdot \vec{\alpha}_0 \cdot \langle \mathbf{u}_0 \rangle_y. \quad (55)$$



The third equation in (15) at low frequencies and the same as averaged to macro-scale is

$$\begin{aligned}\mathbf{u}_0 &= -\frac{1}{\mu} \vec{\mathbf{K}}_0(\mathbf{y}) \cdot \nabla_x p_0(\mathbf{x}) \\ \langle \mathbf{u}_0 \rangle_y &= -\frac{1}{\mu} \left\langle \vec{\mathbf{K}}_0(\mathbf{y}) \right\rangle_y \cdot \nabla_x p_0(\mathbf{x}).\end{aligned}\quad (56)$$

Inserting this to Eq. (55) we obtain

$$\begin{aligned}\nabla_x p_0(\mathbf{x}) \cdot \left\langle \vec{\mathbf{K}}_0^T(\mathbf{y}) \cdot \vec{\mathbf{K}}_0(\mathbf{y}) \right\rangle_y \cdot [\nabla_x p_0(\mathbf{x})]^* &= \\ = [\nabla_x p_0(\mathbf{x})]^* \cdot \left\langle \vec{\mathbf{K}}_0^T(\mathbf{y}) \right\rangle_y \cdot \vec{\mathbf{a}}_0 \cdot \left\langle \vec{\mathbf{K}}_0(\mathbf{y}) \right\rangle_y \cdot \nabla_x p_0(\mathbf{x}).\end{aligned}\quad (57)$$

From Eq. (57) we can obtain the result, indicating the components of the viscous relaxed tortuosity and the static viscous permeability

$$\left\langle \vec{\mathbf{K}}_0^T(\mathbf{y}) \cdot \vec{\mathbf{K}}_0(\mathbf{y}) \right\rangle_y = \left\langle \vec{\mathbf{K}}_0^T(\mathbf{y}) \right\rangle_y \cdot \vec{\mathbf{a}}_0 \cdot \left\langle \vec{\mathbf{K}}_0(\mathbf{y}) \right\rangle_y. \quad (58)$$

For tensor component  $\alpha_{0ij} = \mathbf{e}_i \cdot \vec{\mathbf{a}}_0 \cdot \mathbf{e}_j$ , the above can be presented as

$$\left\langle \left( \vec{\mathbf{K}}_0(\mathbf{y}) \cdot \mathbf{e}_i \right) \cdot \left( \vec{\mathbf{K}}_0(\mathbf{y}) \cdot \mathbf{e}_j \right) \right\rangle_y = \left\langle \mathbf{e}_i \cdot \vec{\mathbf{K}}_0(\mathbf{y}) \cdot \mathbf{e}_i \right\rangle_y \mathbf{e}_i \cdot \vec{\mathbf{a}}_0 \cdot \mathbf{e}_j \left\langle \mathbf{e}_j \cdot \vec{\mathbf{K}}_0(\mathbf{y}) \cdot \mathbf{e}_j \right\rangle_y, \quad (59)$$

from which we obtain [21]

$$\alpha_{0ij} = \frac{\left\langle \left( \vec{\mathbf{K}}_0(\mathbf{y}) \cdot \mathbf{e}_i \right) \cdot \left( \vec{\mathbf{K}}_0(\mathbf{y}) \cdot \mathbf{e}_j \right) \right\rangle_y}{\left\langle \mathbf{e}_i \cdot \vec{\mathbf{K}}_0(\mathbf{y}) \cdot \mathbf{e}_i \right\rangle_y \left\langle \mathbf{e}_j \cdot \vec{\mathbf{K}}_0(\mathbf{y}) \cdot \mathbf{e}_j \right\rangle_y} = \frac{\left\langle K_{0pi}(\mathbf{y}) K_{0pj}(\mathbf{y}) \right\rangle_y}{\left\langle K_{0ii}(\mathbf{y}) \right\rangle_y \left\langle K_{0jj}(\mathbf{y}) \right\rangle_y}, \quad (60)$$

where the Einstein summation notation on  $p$  is implicit: when an index variable (here  $p$ ) appears twice in a single term it implies summation of that term over all the values of the index.

In a principal axes system, cross components of the viscous relaxed tortuosity ( $i \neq j$ ) disappear and we obtain

$$\alpha_{0ii} = \frac{\left\langle \left( \vec{\mathbf{K}}_0(\mathbf{y}) \cdot \mathbf{e}_i \right) \cdot \left( \vec{\mathbf{K}}_0(\mathbf{y}) \cdot \mathbf{e}_i \right) \right\rangle_y}{\left\langle \mathbf{e}_i \cdot \vec{\mathbf{K}}_0(\mathbf{y}) \cdot \mathbf{e}_i \right\rangle_y \left\langle \mathbf{e}_i \cdot \vec{\mathbf{K}}_0(\mathbf{y}) \cdot \mathbf{e}_i \right\rangle_y} = \frac{\left\langle K_{0pi}(\mathbf{y}) K_{0pi}(\mathbf{y}) \right\rangle_y}{\left\langle K_{0ii}(\mathbf{y}) \right\rangle_y^2}, \quad (61)$$

and in isotropic case we have

$$\alpha_0 = \frac{\left\langle K_0^2(\mathbf{y}) \right\rangle_y}{\left\langle K_0(\mathbf{y}) \right\rangle_y^2}. \quad (62)$$

### 8.2.2 Thermal relaxed tortuosity $\alpha'_0$

Multiplying the third equation of (14) by  $T'_0^*$  and averaging this equation over the fluid domain, we obtain (the corresponding boundary condition included)

$$\begin{aligned} j\omega\rho_0c_P\langle T'_0T_0'^* \rangle_y - \kappa'\langle (\nabla_y^2 T'_0)T_0'^* \rangle_y &= j\omega p_0(\mathbf{x})\langle T_0'^* \rangle_y \\ T'_0 &= 0 \text{ at } \Gamma. \end{aligned} \quad (63)$$

Integrating by parts, using Gauss theorem, and utilizing the second line in Eq. (63), the averaged part of the second term in Eq. (63) can be presented as

$$\begin{aligned} \langle (\nabla_y^2 T'_0)T_0'^* \rangle_y &= \langle (\nabla_y \cdot \nabla_y T'_0)T_0'^* \rangle_y = \langle \nabla_y \cdot (T_0'^* \nabla_y T'_0) \rangle_y - \langle (\nabla_y T_0'^*) \cdot (\nabla_y T'_0) \rangle_y = \\ &= \frac{1}{\Omega_f} \oint_{\Gamma+\partial\Omega} T_0'^* \nabla_y T'_0 \cdot \mathbf{e}_n \, dS - \langle (\nabla_y T'_0) \cdot (\nabla_y T_0'^*) \rangle_y = -\langle (\nabla_y T'_0) \cdot (\nabla_y T_0'^*) \rangle_y. \end{aligned} \quad (64)$$

The surface integral vanishes at  $\Gamma$ , due to the boundary conditions in Eq. (63). It vanishes also at  $\partial\Omega$ , due to  $\Omega$ -periodicity of the fields.

Eq. (39), can be presented at low frequencies, according to the second equation in (46), as

$$p_0(\mathbf{x}) = \rho_0c_P \left( \frac{\kappa\phi}{j\omega\rho_0c_P} \overline{K}'_0^{-1} + \alpha'_0 \right) \langle T'_0 \rangle_y = \left( \frac{\kappa\phi}{j\omega} \overline{K}'_0^{-1} + \rho_0c_P\alpha'_0 \right) \langle T'_0 \rangle_y. \quad (65)$$

Eq. (63) can be presented, using Eqs. (64) and (65), as

$$j\omega\rho_0c_P\langle T'_0T_0'^* \rangle_y + \kappa'\langle (\nabla_y T'_0) \cdot (\nabla_y T_0'^*) \rangle_y = \left( \kappa\phi \overline{K}'_0^{-1} + j\omega\rho_0c_P\alpha'_0 \right) \langle T'_0 \rangle_y \langle T_0'^* \rangle_y. \quad (66)$$

The macro-scale static permeabilities and the relaxed tortuosities are real valued. Making the imaginary parts to match in Eq. (66), we obtain

$$\langle T'_0T_0'^* \rangle_y = \alpha'_0 \langle T'_0 \rangle_y \langle T_0'^* \rangle_y. \quad (67)$$

The first equation in (15) at low frequencies and the same as averaged to macro-scale is

$$\begin{aligned} T'_0 &= \frac{1}{\kappa} K'_0(\mathbf{y}) j\omega p_0(\mathbf{x}) \\ \langle T'_0 \rangle_y &= \frac{1}{\kappa} \langle K'_0(\mathbf{y}) \rangle_y j\omega p_0(\mathbf{x}). \end{aligned} \quad (68)$$

Inserting this to Eq. (67) we obtain

$$\langle K_0'^2(\mathbf{y}) \rangle_y = \alpha'_0 \langle K'_0(\mathbf{y}) \rangle_y^2. \quad (69)$$

The thermal relaxed tortuosity can now be written as [9, 8]

$$\alpha'_0 = \frac{\langle K_0'^2(\mathbf{y}) \rangle_y}{\langle K'_0(\mathbf{y}) \rangle_y^2}. \quad (70)$$

### 8.2.3 Viscous tortuosity $\alpha_\infty$

Consider the static field (particle velocity, electric field) in the fluid domain to be constructed of constant external macroscopic static field  $\mathbf{u}_p$  and unrotational field  $-\nabla\phi$  that arises for the total field  $\mathbf{u}$  to fulfil the boundary conditions. The divergence of the total static field is zero. So the corresponding equations are

$$\begin{aligned}\mathbf{u} &= \mathbf{u}_p - \nabla\phi \\ \nabla \cdot \mathbf{u} &= 0 \\ \mathbf{u} \cdot \mathbf{e}_n &= 0 \text{ at } \Gamma.\end{aligned}\tag{71}$$

This is also called an electrical problem because the particle velocity can be substituted by the electric field in which case Eq. (71) describes an electrical conduction problem for a porous medium filled with a conducting fluid and having an insulating solid phase [9, 11].

Averaging over the fluid domain, the equations are

$$\begin{aligned}\langle \mathbf{u} \rangle_y &= \mathbf{u}_p - \langle \nabla\phi \rangle_y \\ \nabla \cdot \mathbf{u} &= 0 \\ \mathbf{u} \cdot \mathbf{e}_n &= 0 \text{ at } \Gamma.\end{aligned}\tag{72}$$

At high frequencies, Eq. (27) can be written as

$$\nabla_x p_0(\mathbf{x}) = -j\omega\rho_0 \vec{\alpha}_\infty \cdot \langle \mathbf{u}_0 \rangle_y,\tag{73}$$

where  $\vec{\alpha}_\infty$  is the limiting value of the dynamic viscous tortuosity when the frequency grows to infinite. It can be presented as a sum of the identic dyadic and a deviation of that as [9]

$$\vec{\alpha}_\infty = (\vec{\mathbf{I}} + \vec{\chi}_\infty).\tag{74}$$

At very high frequencies there are no viscous effects and in that case we can write

$$\nabla_x p_0(\mathbf{x}) = -j\omega\rho_0 \mathbf{u}_p(\mathbf{x})\tag{75}$$

and Eq. (73) can be written as

$$\mathbf{u}_p(\mathbf{x}) = \vec{\alpha}_\infty \cdot \langle \mathbf{u}_0 \rangle_y = (\vec{\mathbf{I}} + \vec{\chi}_\infty) \cdot \langle \mathbf{u}_0 \rangle_y.\tag{76}$$

This can be presented, including the properties of  $\mathbf{u}$ , as

$$\begin{aligned}\langle \mathbf{u}_0 \rangle_y &= \mathbf{u}_p(\mathbf{x}) - \vec{\chi}_\infty \cdot \langle \mathbf{u}_0 \rangle_y \\ \nabla \cdot \mathbf{u}_0 &= 0 \\ \mathbf{u}_0 \cdot \mathbf{e}_n &= 0 \text{ at } \Gamma.\end{aligned}\tag{77}$$

It can be seen that the equations above are the same as in Eq. (72) if  $\mathbf{u}_0$  corresponds the term  $\mathbf{u}$  and  $\vec{\chi}_\infty \cdot \langle \mathbf{u}_0 \rangle_y$  corresponds the term  $\langle \nabla\phi \rangle_y$ . So, solving the static problem of (71), the dynamic viscous tortuosity at high frequencies can be obtained from

$$\begin{aligned}\mathbf{u}_p &= \vec{\alpha}_\infty \cdot \langle \mathbf{u} \rangle_y \\ \vec{\alpha}_\infty^{-1} \cdot \mathbf{u}_p &= \langle \mathbf{u} \rangle_y.\end{aligned}\quad (78)$$

Let  $\mathbf{u}_p^{(i)}$  be the static external field in case  $i$  (e.g.,  $i = 1, 2, 3$  for field in the direction of  $x, y$  and  $z$  axes), and  $\mathbf{u}^{(i)}$  and  $\phi^{(i)}$  be the corresponding total field and the potential. In that case we obtain

$$\mathbf{u}_p^{(i)} \cdot \vec{\alpha}_\infty^{-1} \cdot \mathbf{u}_p^{(j)} = \langle \mathbf{u}_p^{(i)} \cdot \mathbf{u}^{(j)} \rangle_y = \langle \mathbf{u}^{(i)} \cdot \mathbf{u}^{(j)} \rangle_y + \langle \nabla \phi^{(i)} \cdot \mathbf{u}^{(j)} \rangle_y. \quad (79)$$

Integrating by parts, using Gauss theorem, and utilizing the second and third line in Eq. (71), the last term in the equation above can be seen to vanish

$$\begin{aligned}\langle \nabla \phi^{(i)} \cdot \mathbf{u}^{(j)} \rangle_y &= \langle \nabla \cdot (\phi^{(i)} \mathbf{u}^{(j)}) \rangle_y - \langle \phi^{(i)} \nabla \cdot \mathbf{u}^{(j)} \rangle_y = \langle \nabla \cdot (\phi^{(i)} \mathbf{u}^{(j)}) \rangle_y \\ &= \frac{1}{\Omega_f} \oint_{\Gamma + \partial\Omega} \phi^{(i)} \mathbf{u}^{(j)} \cdot \mathbf{e}_n \, dS = 0.\end{aligned}\quad (80)$$

The surface integral vanishes at  $\Gamma$ , due to the boundary conditions in Eq. (71). It vanishes also at  $\partial\Omega$ , due to  $\Omega$ -periodicity of the fields.

So from Eq. (79) we obtain the formula giving the viscous tortuosity dyadic at high frequencies

$$\mathbf{u}_p^{(i)} \cdot \vec{\alpha}_\infty^{-1} \cdot \mathbf{u}_p^{(j)} = \langle \mathbf{u}_p^{(i)} \cdot \mathbf{u}^{(j)} \rangle_y = \langle \mathbf{u}^{(i)} \cdot \mathbf{u}^{(j)} \rangle_y. \quad (81)$$

If the absolute value of the macroscopic external field is unity ( $|\mathbf{u}_p| = 1$ ), we obtain for the tensor components of the viscous tortuosity [9]

$$\alpha_{\infty ij}^{-1} = \mathbf{u}_p^{(i)} \cdot \vec{\alpha}_\infty^{-1} \cdot \mathbf{u}_p^{(j)} = \langle \mathbf{u}_p^{(i)} \cdot \mathbf{u}^{(j)} \rangle_y = \langle \mathbf{u}^{(i)} \cdot \mathbf{u}^{(j)} \rangle_y. \quad (82)$$

In a principal axes system, cross components disappear and we have

$$\langle \mathbf{u}^{(i)} \cdot \mathbf{u}^{(i)} \rangle_y = \mathbf{u}_p^{(i)} \cdot \vec{\alpha}_\infty^{-1} \cdot \mathbf{u}_p^{(i)} = \alpha_{\infty ii}^{-1} \alpha_{\infty ii}^{-1} \mathbf{u}_p^{(i)} \cdot \alpha_{\infty ii}^{-1} \mathbf{u}_p^{(i)} = \alpha_{\infty ii} \langle \mathbf{u}^{(i)} \rangle_y \cdot \langle \mathbf{u}^{(i)} \rangle_y, \quad (83)$$

from which we obtain

$$\alpha_{\infty ii} = \frac{\langle \mathbf{u}^{(i)} \cdot \mathbf{u}^{(i)} \rangle_y}{\langle \mathbf{u}^{(i)} \rangle_y \cdot \langle \mathbf{u}^{(i)} \rangle_y}. \quad (84)$$

In the isotropic case this leads to

$$\alpha_\infty = \frac{\langle \mathbf{u} \cdot \mathbf{u} \rangle_y}{\langle \mathbf{u} \rangle_y \cdot \langle \mathbf{u} \rangle_y}. \quad (85)$$

## 8.2.4 Thermal tortuosity $\alpha'_\infty$

From Eq. (39), we obtain at high frequencies

$$p_0(\mathbf{x}) = \rho_0 c_p \alpha'_\infty \langle T'_0 \rangle_y. \quad (86)$$

The third equation in (14) at high frequencies, averaged over the fluid volume, is

$$p_0(\mathbf{x}) = \rho_0 c_p \langle T_0' \rangle_y. \quad (87)$$

Comparing the equations above, we see that the thermal tortuosity at high frequencies is one

$$\alpha'_\infty = 1. \quad (88)$$

### 8.2.5 Viscous characteristic length

If the divergence of the particle velocity disappears, the viscous stress dyadic in Eq. (2) is

$$\vec{\sigma}_\mu = \mu [\nabla \mathbf{u} + (\nabla \mathbf{u})^T]. \quad (89)$$

Viscous loss power per unit volume can be obtained from [16]

$$W_v = -(\nabla \cdot \vec{\sigma}_\mu) \cdot \mathbf{u}. \quad (90)$$

By integrating over volume  $\Omega_f$ , the average viscous loss power per unit volume can be seen to be

$$\begin{aligned} \langle W_v \rangle &= -\frac{1}{\Omega_f} \int_{\Omega_f} (\nabla \cdot \vec{\sigma}_\mu) \cdot \mathbf{u} d\Omega = -\frac{1}{\Omega_f} \int_{\Omega_f} \nabla \cdot (\vec{\sigma}_\mu \cdot \mathbf{u}) d\Omega + \int_{\Omega_f} (\vec{\sigma}_\mu \cdot \nabla \mathbf{u}) : \hat{\mathbf{I}} d\Omega = \\ &= -\frac{1}{\Omega_f} \oint_{\Gamma + \partial\Omega} \mathbf{e}_n \cdot (\vec{\sigma}_\mu \cdot \mathbf{u}) dS + \int_{\Omega_f} (\vec{\sigma}_\mu \cdot \nabla \mathbf{u}) : \hat{\mathbf{I}} d\Omega = \\ &= \frac{\mu}{\Omega_f} \int_{\Omega_f} \{[\nabla \mathbf{u} + (\nabla \mathbf{u})^T] \cdot \nabla \mathbf{u}\} : \hat{\mathbf{I}} d\Omega, \end{aligned} \quad (91)$$

where the partial integration, the Gauss theorem and Eq. (89) have been used. The surface integral vanishes at  $\partial\Omega$ , due to  $\Omega$ -periodicity of the fields. It vanishes also at  $\Gamma$ , because the particle velocity vanishes at  $\Gamma$ . The normal component of it vanishes naturally, and the tangential component vanishes according to the next equation.

The viscosity causes a boundary layer near surfaces. Near a plane surface the particle velocity is, due to this effect, (see, e.g., [19, 16] and Figure 7)

$$\mathbf{u}(\mathbf{r}) = \mathbf{u}_p(\mathbf{r}_w) (1 - e^{-(1+j)\xi/\delta}), \quad (92)$$

where  $\mathbf{r}_w$  and  $\mathbf{r}$  are coordinates on the surface and above it at a normal distance of  $\xi$  from the surface. The particle velocity  $\mathbf{u}$  near the surface is tangential to the surface and it vanishes just on it. The particle velocity  $\mathbf{u}_p$  is the velocity without this viscous surface effect. At high frequencies, the different particle velocities are equal except in the very close vicinity of the surface.

Now the viscous effects near boundaries can be taken into account using Eq. (92) if the surface is assumed to be locally plane. With it, the integrand in (91) only contains term (in complex notation with time harmonic fields)

$$\{[\nabla \mathbf{u} + (\nabla \mathbf{u})^T] \cdot (\nabla \mathbf{u})^*\} : \hat{\mathbf{I}} = \frac{\partial u}{\partial \xi} \left( \frac{\partial u}{\partial \xi} \right)^* \quad (93)$$

and the average viscous loss power per unit volume is

$$\begin{aligned}
 \langle W_v \rangle &= \frac{\mu}{\Omega_f} \int_{\Omega} \frac{\partial u(\mathbf{r})}{\partial \xi} \left( \frac{\partial u(\mathbf{r})}{\partial \xi} \right)^* d\Omega \approx \frac{\mu}{\Omega_f} \frac{2}{\delta_v^2} \int_{\Gamma} |u_p(\mathbf{r}_w)|^2 \int_{\xi} e^{-2\xi/\delta} d\xi d\Gamma = \\
 &= \frac{\mu}{\Omega_f \delta} \int_{\Gamma} |u_p(\mathbf{r}_w)|^2 d\Gamma.
 \end{aligned} \tag{94}$$

With a plane wave, the acoustic energy density is

$$E = \rho_0 |u|^2. \tag{95}$$

At high frequencies, the thermal tortuosity  $\alpha_{\infty}'$  is one, according to Eq. (88), and the normalized effective compressibility  $\beta$  is one, according to Eq. (40). Thus in the isotropic case at high frequencies, according to Eq. (41),

$$\begin{aligned}
 c_{eff} &= \frac{c_0}{\sqrt{\alpha}} \\
 k &= \frac{\omega \sqrt{\alpha}}{c_0}.
 \end{aligned} \tag{96}$$

With a plane wave, the acoustic intensity  $I$  is the acoustic energy density times the speed of sound, which at high frequencies is, according to Eqs. (95) and (96)

$$I = \rho_0 \frac{c_0}{\sqrt{\alpha}} |u|^2. \tag{97}$$

The average acoustic intensity at high frequencies with a plane wave is thus

$$\langle I \rangle = \frac{\rho_0 c_0}{\Omega_f \sqrt{\alpha_{\infty}}} \int_{\Omega_f} |u(\mathbf{r})|^2 d\Omega \approx \frac{\rho_0 c_0}{\Omega_f \sqrt{\alpha_{\infty}}} \int_{\Omega_f} |u_p(\mathbf{r})|^2 d\Omega. \tag{98}$$

In the last formula, the surface effect has been ignored. At high frequencies it is reasonable.

The imaginary part of the wave number, attached to attenuation of sound due to viscosity, can be presented as [19]

$$\text{Im}\{k\} = -\frac{\langle W_v \rangle}{2\langle I \rangle}. \tag{99}$$

With a plane wave at high frequencies, it can be presented, using Eqs. (94), (98) and (49), as

$$\text{Im}\{k\} = -\frac{\mu \sqrt{\alpha_{\infty}}}{2\delta \rho_0 c_0} \frac{\int_{\Gamma} |u_p(\mathbf{r}_w)|^2 d\Gamma}{\int_{\Omega_f} |u_p(\mathbf{r})|^2 d\Omega} = -\sqrt{\frac{\mu \omega \alpha_{\infty}}{2\rho_0}} \frac{1}{2c_0} \frac{\int_{\Gamma} |u_p(\mathbf{r}_w)|^2 d\Gamma}{\int_{\Omega_f} |u_p(\mathbf{r})|^2 d\Omega}. \tag{100}$$

At high frequencies, the viscous tortuosity can be given as [19]

$$\lim\{\alpha(\omega)\} = \alpha_{\infty} + C \left( \frac{1}{j\omega} \right)^p, \quad \omega \rightarrow \infty. \tag{101}$$

The imaginary part of the wave number at high frequencies is thus, utilizing also Eq. (96) (lower),

$$\begin{aligned}
 \text{Im}\{k\} &= \text{Im}\left\{\omega \frac{\sqrt{\alpha(\omega)}}{c_0}\right\} = \\
 &= \text{Im}\left\{\omega \frac{\sqrt{\alpha_\infty + C\left(\frac{1}{j\omega}\right)^p}}{c_0}\right\} \approx \text{Im}\left\{\omega \frac{\sqrt{\alpha_\infty}\left[1 + \frac{C}{2\alpha_\infty}\left(\frac{1}{j\omega}\right)^p\right]}{c_0}\right\} = \\
 &= \frac{C}{2c_0\sqrt{\alpha_\infty}} \omega^{1-p} \text{Im}\{j^{-p}\}.
 \end{aligned} \tag{102}$$

Comparing this to the frequency dependence of Eq. (100), it can be noticed that  $p = \frac{1}{2}$  and

$$\begin{aligned}
 \text{Im}\{k\} &= \frac{C}{2c_0} \sqrt{\frac{\omega}{\alpha_\infty}} \text{Im}\left\{\frac{1}{\sqrt{j}}\right\} = \frac{C}{2c_0} \sqrt{\frac{\omega}{\alpha_\infty}} \text{Im}\left\{\frac{1-j}{\sqrt{2}}\right\} = \\
 &= -\frac{C}{2c_0} \sqrt{\frac{\omega}{2\alpha_\infty}}.
 \end{aligned} \tag{103}$$

From this we can further obtain, by using Eq. (100)

$$C = -2c_0 \sqrt{\frac{2\alpha_\infty}{\omega}} \text{Im}\{k\} = \alpha_\infty \sqrt{\frac{\mu}{\rho_0}} \frac{\int_{\Gamma} |u_p(\mathbf{r}_w)|^2 d\Gamma}{\int_{\Omega_f} |u_p(\mathbf{r})|^2 d\Omega}. \tag{104}$$

Eq. (101) can now be presented, utilizing Eq. (49), as

$$\lim\{\alpha(\omega)\} = \alpha_\infty \left[ 1 + \frac{\sqrt{\frac{\mu}{j\rho_0\omega}} \int_{\Gamma} |u_p(\mathbf{r}_w)|^2 d\Gamma}{\int_{\Omega_f} |u_p(\mathbf{r})|^2 d\Omega} \right] = \alpha_\infty \left[ 1 + (1-j) \frac{\delta}{\Lambda} \right], \quad \omega \rightarrow \infty, \tag{105}$$

where, according to definition (48) (first line),  $\Lambda$  is the viscous characteristic length [19], being

$$\Lambda = 2 \frac{\int_{\Omega_f} |u_p(\mathbf{r})|^2 d\Omega}{\int_{\Gamma} |u_p(\mathbf{r}_w)|^2 d\Gamma}. \tag{106}$$

So, the viscous characteristic length has been presented by the volume and surface integrals of the squared particle velocity without viscous losses.

The problem was assumed to be isotropic. Using Ref. [9], it can be deduced that in the anisotropic case the viscous characteristic length can be obtained from

$$2\bar{\Lambda}^{-1} = \bar{\mathbf{a}}_{\infty} \cdot \bar{\mathbf{U}}, \quad (107)$$

where the components of the inverse of the viscous tortuosity  $\bar{\mathbf{a}}_{\infty}$  can be obtained from Eq. (82) and the components of  $\bar{\mathbf{U}}$  can be obtained from

$$U_{ij} = \mathbf{e}_i \cdot \bar{\mathbf{U}} \cdot \mathbf{e}_j = \frac{1}{\Omega_f} \int_{\Gamma} \mathbf{u}^{(i)} \cdot \mathbf{u}^{(j)} d\Gamma. \quad (108)$$

The symbols  $\mathbf{u}^{(i)}$  are the same as in paragraph 8.2.3 and calculated as presented there.

In a principal axes system, cross components disappear and we have

$$\Lambda_{ii} = 2 \frac{\int_{\Omega_f} \mathbf{u}^{(i)} \cdot \mathbf{u}^{(i)} d\Omega}{\int_{\Gamma} \mathbf{u}^{(i)} \cdot \mathbf{u}^{(i)} d\Gamma}. \quad (109)$$

### 8.2.6 Thermal characteristic length

The thermal conductivity causes a boundary layer near surfaces. Near a plane surface the temperature is, due to this effect, (see, e.g., [20, 16], Figure 7 is also valid for temperature near a plane surface)

$$T'_0(\mathbf{r}) = T'_{00}(\mathbf{r}_w) \left(1 - e^{-(1+j)\xi/\delta'}\right), \quad (110)$$

where  $\mathbf{r}_w$  and  $\mathbf{r}$  are coordinates on the surface and above it at a normal distance of  $\xi$  from the surface, and  $T'_{00}$  is the temperature without the boundary effects. At high frequencies, according to the third equation in (14),  $T'_{00}$  is not a function of the micro-scale coordinates. So at high frequencies

$$\begin{aligned} \lim \left\{ \langle T'_0(\mathbf{r}) \rangle \right\} &= \frac{T'_{00}}{\Omega_f} \int_{\Omega_f} \left(1 - e^{-(1+j)\xi/\delta'}\right) d\Omega = T'_{00} \left[ 1 - \frac{1}{\Omega_f} \int_{\Gamma} \int_{\xi} \left(e^{-(1+j)\xi/\delta'}\right) d\xi d\Gamma \right] = \\ &= T'_{00} \left[ 1 - \frac{1}{\Omega_f} \int_{\Gamma} \int_{\xi} \left(e^{-(1+j)\xi/\delta'}\right) d\xi d\Gamma \right] = T'_{00} \left[ 1 - \frac{1-j}{2} \delta' \frac{1}{\Omega_f} \int_{\Gamma} d\Gamma \right] = \\ &= T'_{00} \left[ 1 - (1-j) \frac{\delta'}{\Lambda'} \right], \quad \omega \rightarrow \infty, \end{aligned} \quad (111)$$

where, according to definition (48) (second line),  $\Lambda'$  is the thermal characteristic length [20], being

$$\Lambda' = 2 \frac{\Omega_f}{\Gamma} = 2 \frac{\int d\Omega}{\int_{\Gamma} d\Gamma}. \quad (112)$$

### 8.2.7 Dynamic tortuosity and compressibility

The dynamic viscous tortuosity  $\alpha(\omega)$  in the isotropic case, according to Pride *et al.* [22], and the normalized dynamic effective compressibility  $\beta(\omega)$ , according to Lafarge [23, 9], can now be approximated by (see also Eq. (40))



$$\alpha(\omega) = \alpha_\infty + \frac{f(\zeta)}{j\zeta}$$

$$\beta(\omega) = \gamma - \frac{\gamma-1}{\alpha'(\omega)} \quad \alpha'(\omega) = 1 + \frac{f'(\zeta')}{j\zeta'},$$
(113)

where

$$f(\zeta) = 1 - q + q \sqrt{1 + j \frac{2\zeta(\alpha_0 - \alpha_\infty)}{q}}$$

$$f'(\zeta') = 1 - q' + q' \sqrt{1 + j \frac{2\zeta'(\alpha'_0 - 1)}{q'}}$$

$$\zeta = \frac{\omega \rho_0 \bar{K}_0}{\mu \phi} \quad \zeta' = \frac{\omega \rho_0 c_P \bar{K}'_0}{\kappa \phi}$$

$$q = \frac{2}{\phi} \frac{\bar{K}_0 \left( \frac{\alpha_\infty}{\Lambda} \right)^2}{\alpha_0 - \alpha_\infty} \quad q' = \frac{2}{\phi} \frac{\bar{K}'_0 \left( \frac{1}{\Lambda'} \right)^2}{\alpha'_0 - 1}.$$
(114)

This is called “Johnson-Champoux-Allard-Pride-Lafarge” (JCAPL) model [13, 21]. If  $q = q' = 1$ , the equations lead to “Johnson-Champoux-Allard-Lafarge” (JCAL) model where the relaxed tortuosities  $\alpha_0$  and  $\alpha'_0$  are not used as independent variables [7, 13, 21, 24]. In that case, terms  $\alpha_0 - \alpha_\infty$  and  $\alpha'_0 - 1$  in the expressions of  $f(\zeta)$  and  $f'(\zeta')$  are replaced by

$$\alpha_0 - \alpha_\infty = \frac{2\bar{K}_0}{\phi} \left( \frac{\alpha_\infty}{\Lambda} \right)^2$$

$$\alpha'_0 - 1 = \frac{2\bar{K}'_0}{\phi} \left( \frac{1}{\Lambda'} \right)^2.$$
(115)

If, in addition [21],

$$\bar{K}'_0 = \frac{\phi \Lambda'^2}{8},$$
(116)

the equations lead to “Johnson-Champoux-Allard” (JCA) model, in which the thermal permeability  $\bar{K}'_0$  is not used as an independent variable, and the term  $\alpha'_0 - 1$  in the expression of  $f'(\zeta')$  is replaced by

$$\alpha'_0 - 1 = \frac{1}{4}.$$
(117)

In the anisotropic case, the dynamic viscous tortuosity  $\vec{\alpha}(\omega)$  can be obtained from the generalization of  $\alpha(\omega)$  from Eqs. (113) and (114) as [9]

$$\vec{\alpha}(\omega) = \vec{\alpha}_\infty - j\zeta^{-1} \cdot \vec{f}(\zeta),$$
(118)

where

$$\begin{aligned}\vec{f}(\vec{\zeta}) &= \vec{I} - \vec{q} + \vec{q} \cdot \sqrt{\vec{I} + j2\vec{q}^{-1} \cdot \vec{\zeta} \cdot (\vec{a}_0 - \vec{a}_\infty)} \\ \vec{\zeta} &= \frac{\omega \rho_0}{\mu \phi} \vec{K}_0\end{aligned}\quad (119)$$

$$\vec{q} = \frac{2}{\phi} \vec{K}_0 \cdot \left( \vec{\Lambda}^{-1} \cdot \vec{a}_\infty \right)^2 \cdot (\vec{a}_0 - \vec{a}_\infty)^{-1}.$$

If  $\vec{q} = \vec{I}$  and  $q' = 1$ , the equations lead to “Johnson-Champoux-Allard-Lafarge” (JCAL) model as in the isotropic case. In that case, term  $\alpha_0' - 1$  in the expression of  $f(\zeta')$  is as in Eq. (115) and  $\vec{a}_0 - \vec{a}_\infty$  in the expression of  $\vec{f}(\vec{\zeta})$  is replaced by

$$\vec{a}_0 - \vec{a}_\infty = \frac{2}{\phi} \vec{K}_0 \cdot \left( \vec{\Lambda}^{-1} \cdot \vec{a}_\infty \right)^2. \quad (120)$$

In the “Johnson-Champoux-Allard” (JCA) model, the replaced expression for  $\alpha_0' - 1$  in the expression of  $f(\zeta')$  is as in the isotropic case, Eq. (117).

Lafarge [9] uses a different formula for  $\vec{q}$ . Taking the inverse of  $\vec{q}$  above we obtain

$$\vec{q}^{-1} = \frac{\phi}{2} (\vec{a}_0 - \vec{a}_\infty) \cdot \left[ \vec{K}_0 \cdot \left( \vec{\Lambda}^{-1} \cdot \vec{a}_\infty \right)^2 \right]^{-1}, \quad (121)$$

from which we obtain

$$\frac{2}{\phi} (\vec{a}_0 - \vec{a}_\infty)^{-1} \cdot \vec{q} \cdot \vec{K}_0 \cdot \left( \vec{\Lambda}^{-1} \cdot \vec{a}_\infty \right)^2 = \vec{I}. \quad (122)$$

Now we can write

$$\begin{aligned}\sqrt{\frac{2}{\phi} \vec{q}^{-1} \cdot \vec{K}_0 \cdot (\vec{a}_0 - \vec{a}_\infty)} &= \sqrt{\frac{2}{\phi} \vec{q}^{-1} \cdot \vec{K}_0 \cdot (\vec{a}_0 - \vec{a}_\infty) \cdot \vec{I}} \\ &= \sqrt{\frac{2}{\phi} \vec{q}^{-1} \cdot \vec{K}_0 \cdot (\vec{a}_0 - \vec{a}_\infty) \cdot \frac{2}{\phi} (\vec{a}_0 - \vec{a}_\infty)^{-1} \cdot \vec{q} \cdot \vec{K}_0 \cdot \left( \vec{\Lambda}^{-1} \cdot \vec{a}_\infty \right)^2} \\ &= \sqrt{\left( \frac{2}{\phi} \right)^2 \left( \vec{q}^{-1} \cdot \vec{K}_0 \right)^2 \cdot \left( \vec{\Lambda}^{-1} \cdot \vec{a}_\infty \right)^2} = \frac{2}{\phi} \vec{q}^{-1} \cdot \vec{K}_0 \cdot \vec{\Lambda}^{-1} \cdot \vec{a}_\infty.\end{aligned}\quad (123)$$

From the equation above we obtain the formula of Lafarge [9], used to solve  $\vec{q}$

$$\sqrt{\frac{2}{\phi} \vec{q}^{-1} \cdot \vec{K}_0 \cdot (\vec{a}_0 - \vec{a}_\infty)} = \frac{2}{\phi} \vec{q}^{-1} \cdot \vec{K}_0 \cdot \vec{\Lambda}^{-1} \cdot \vec{a}_\infty. \quad (124)$$

Once the dynamic tortuosities and the effective compressibility have been calculated, the impedance, the effective sound speed and the wave number vector can be calculated with rigid frame models from the same equations, Eq. (41), as with the direct calculation method.

## 9. Biot model

In the Biot model, the elastic behaviour of the frame is taken into account, leading to equations with three wave motions, two compressional waves and one shear wave, all of them propagating both in the air and the solid phase. The viscous and thermal effects are coupled, so the logic presented earlier for the rigid frame models cannot be directly applied [9]. The impedance, the complex sound speed and the complex wave number cannot now be obtained using Eq. (41), using the effective density  $\vec{\rho}_{\text{eff}}$  or its normalized version dynamic viscous tortuosity  $\vec{\alpha}(\omega)$ , Eqs. (26) and (28), and the effective compressibility  $Q_{\text{eff}}$  or its normalized form  $\beta$ , Eq. (37). However, these parameters can directly be included in the parameters of the Biot model, as is presented in the following, to take into account the viscous and thermal properties of the fluid phase. The effective density and the effective compressibility, used in the Biot parameters, can be based on either the direct numerical approach or any of the methods in the hybrid numerical approach.

The internal losses of the solid phase can be taken into account in a familiar way using complex elastic parameters of the viscoelastic structure.

### 9.1 Stress-strain relationships

In the Biot model, the stress–strain relationships are [9, 20]

$$\begin{aligned}\vec{\sigma}_s &= [(P - 2N)\vec{e}_s : \vec{\mathbf{I}} + Q\vec{e}_f : \vec{\mathbf{I}}]\vec{\mathbf{I}} + 2N\vec{e}_s \\ \vec{\sigma}_f &= -\phi p\vec{\mathbf{I}} = (Q\vec{e}_s : \vec{\mathbf{I}} + R\vec{e}_f : \vec{\mathbf{I}})\vec{\mathbf{I}},\end{aligned}\quad (125)$$

where  $\vec{\sigma}$  is the stress dyadic,  $\vec{e}$  is the strain dyadic,  $\vec{e} : \vec{\mathbf{I}}$  is the dilatation

$$\begin{aligned}\vec{e} &= \frac{1}{2}[\nabla\mathbf{s} + (\nabla\mathbf{s})^T] \\ \vec{e} : \vec{\mathbf{I}} &= \nabla \cdot \mathbf{s},\end{aligned}\quad (126)$$

where  $\mathbf{s}$  is the displacement vector, and subscripts “s” and “f” refer to the solid phase and the fluid phase correspondingly.

Quantity  $N$  is the shear modulus of the frame in vacuum. Other parameters  $P$ ,  $Q$  and  $R$  can be obtained from

$$\begin{aligned}P &= B[(1 - \phi)A + \phi K_b Q_{\text{eff}}] + \frac{4}{3}N \\ Q &= BA\phi \\ R &= B\phi^2,\end{aligned}\quad (127)$$

where

$$\begin{aligned}A &= 1 - \phi - \frac{K_b}{K_s} \\ B &= \frac{K_s}{A + \phi K_s Q_{\text{eff}}},\end{aligned}\quad (128)$$

and where  $K_b$  and  $K_s$  are the bulk moduli of the frame in vacuum and the elastic solid from which the frame is made.

For materials used in practice,  $K_s \gg K_b$  and  $K_s \gg 1/Q_{\text{eff}}$ , in which case we have

$$\begin{aligned} A &= 1 - \phi \\ B &= \frac{1}{\phi Q_{\text{eff}}}, \end{aligned} \quad (129)$$

and

$$\begin{aligned} P &= \frac{(1 - \phi)^2}{\phi Q_{\text{eff}}} + K_b + \frac{4}{3}N \\ Q &= \frac{1 - \phi}{Q_{\text{eff}}} \\ R &= \frac{\phi}{Q_{\text{eff}}}. \end{aligned} \quad (130)$$

In that case the bulk modulus  $K_s$  of the elastic solid is not needed.

## 9.2 Equations of motion

As well in the Biot model, the equations of motion are [9, 20]

$$\begin{aligned} \nabla \cdot \vec{\sigma}_s &= \vec{\rho}_{11} \cdot \frac{\partial^2 \mathbf{s}_s}{\partial t^2} + \vec{\rho}_{12} \cdot \frac{\partial^2 \mathbf{s}_f}{\partial t^2} \\ \nabla \cdot \vec{\sigma}_f &= \vec{\rho}_{21} \cdot \frac{\partial^2 \mathbf{s}_s}{\partial t^2} + \vec{\rho}_{22} \cdot \frac{\partial^2 \mathbf{s}_f}{\partial t^2}, \end{aligned} \quad (131)$$

where

$$\begin{aligned} \vec{\rho}_{11} &= \rho_1 \vec{\mathbf{I}} + \phi \rho_0 (\vec{\mathbf{a}}(\omega) - \vec{\mathbf{I}}) \\ \vec{\rho}_{12} &= \vec{\rho}_{21} = -\phi \rho_0 (\vec{\mathbf{a}}(\omega) - \vec{\mathbf{I}}) \\ \vec{\rho}_{22} &= \phi \rho_0 \vec{\mathbf{a}}(\omega), \end{aligned} \quad (132)$$

where  $\rho_1$  is the density of the frame in vacuum

$$\rho_1 = (1 - \phi)\rho_s, \quad (133)$$

where  $\rho_s$  is the density of the elastic solid from which the frame is made.

## 9.3 Biot equations

By combining Eqs. (125) and (131) we obtain the ‘‘Biot Equations’’

$$\begin{aligned}
 \vec{\rho}_{11} \cdot \frac{\partial^2 \mathbf{s}_s}{\partial t^2} + \vec{\rho}_{12} \cdot \frac{\partial^2 \mathbf{s}_f}{\partial t^2} &= P \nabla (\vec{\mathbf{e}}_s : \vec{\mathbf{I}}) + Q \nabla (\vec{\mathbf{e}}_f : \vec{\mathbf{I}}) - N \nabla \times \nabla \times \mathbf{s}_s \\
 \vec{\rho}_{12} \cdot \frac{\partial^2 \mathbf{s}_s}{\partial t^2} + \vec{\rho}_{22} \cdot \frac{\partial^2 \mathbf{s}_f}{\partial t^2} &= Q \nabla (\vec{\mathbf{e}}_s : \vec{\mathbf{I}}) + R \nabla (\vec{\mathbf{e}}_f : \vec{\mathbf{I}}),
 \end{aligned} \tag{134}$$

where the following relationship has been utilized by the help of Eq. (126)

$$\begin{aligned}
 \nabla \cdot [\vec{\mathbf{e}} - (\vec{\mathbf{e}} : \vec{\mathbf{I}}) \vec{\mathbf{I}}] &= \frac{1}{2} \nabla \cdot [\nabla \mathbf{s} + (\nabla \mathbf{s})^T] - \nabla (\nabla \cdot \mathbf{s}) \\
 &= \frac{1}{2} \nabla \cdot [\nabla \mathbf{s} + (\nabla \mathbf{s})^T] - \nabla \cdot (\nabla \mathbf{s})^T = \frac{1}{2} \nabla \cdot [\nabla \mathbf{s} - (\nabla \mathbf{s})^T] \\
 &= -\frac{1}{2} \nabla \cdot [(\nabla \times \mathbf{s}) \times \vec{\mathbf{I}}] = -\frac{1}{2} \nabla \times \nabla \times \mathbf{s}.
 \end{aligned} \tag{135}$$

Biot Equations (134) can be presented in time harmonic fields as

$$-\omega^2 \begin{bmatrix} \vec{\rho}_{11} & \vec{\rho}_{12} \\ \vec{\rho}_{12} & \vec{\rho}_{22} \end{bmatrix} \cdot \begin{bmatrix} \mathbf{s}_s \\ \mathbf{s}_f \end{bmatrix} = \begin{bmatrix} P & Q \\ Q & R \end{bmatrix} \nabla \begin{bmatrix} \vec{\mathbf{e}}_s : \vec{\mathbf{I}} \\ \vec{\mathbf{e}}_f : \vec{\mathbf{I}} \end{bmatrix} - \begin{bmatrix} N \nabla \times \nabla \times \mathbf{s}_s \\ 0 \end{bmatrix}. \tag{136}$$

The displacements can be divided into the compressional waves (second subscript “c”) and the shear waves (second subscript “s”), the first being irrotational and the second divergence-free, obeying

$$\begin{aligned}
 \mathbf{s}_s &= \mathbf{s}_{sc} + \mathbf{s}_{ss} & \mathbf{s}_f &= \mathbf{s}_{fc} + \mathbf{s}_{fs} \\
 \nabla \times \mathbf{s}_{sc} &= 0 & \nabla \cdot \mathbf{s}_{ss} &= 0 \\
 \nabla \times \mathbf{s}_{fc} &= 0 & \nabla \cdot \mathbf{s}_{fs} &= 0.
 \end{aligned} \tag{137}$$

With this division, Eqs. (136) can be presented separately for the compressional waves as

$$-\omega^2 \begin{bmatrix} \vec{\rho}_{11} & \vec{\rho}_{12} \\ \vec{\rho}_{12} & \vec{\rho}_{22} \end{bmatrix} \cdot \begin{bmatrix} \mathbf{s}_{sc} \\ \mathbf{s}_{fc} \end{bmatrix} = \begin{bmatrix} P & Q \\ Q & R \end{bmatrix} \nabla^2 \begin{bmatrix} \mathbf{s}_{sc} \\ \mathbf{s}_{fc} \end{bmatrix} \tag{138}$$

and for the shear waves as

$$-\omega^2 \begin{bmatrix} \vec{\rho}_{11} & \vec{\rho}_{12} \\ \vec{\rho}_{12} & \vec{\rho}_{22} \end{bmatrix} \cdot \begin{bmatrix} \mathbf{s}_{ss} \\ \mathbf{s}_{fs} \end{bmatrix} = \begin{bmatrix} N \nabla^2 \mathbf{s}_{ss} \\ 0 \end{bmatrix}. \tag{139}$$

The stress-strain relationships in Eq. (125) can be presented for later purposes only for the compressional waves as

$$\begin{aligned}
 \vec{\boldsymbol{\sigma}}_{sc} &= [P \vec{\mathbf{e}}_{sc} : \vec{\mathbf{I}} + Q \vec{\mathbf{e}}_{fc} : \vec{\mathbf{I}}] \vec{\mathbf{I}} \\
 -\phi p &= (Q \vec{\mathbf{e}}_{sc} : \vec{\mathbf{I}} + R \vec{\mathbf{e}}_{fc} : \vec{\mathbf{I}}),
 \end{aligned} \tag{140}$$

which can be presented by the help of Eq. (126) also as

$$\begin{aligned}
 \vec{\boldsymbol{\sigma}}_{sc} &= [P \nabla \cdot \mathbf{s}_{sc} + Q \nabla \cdot \mathbf{s}_{fc}] \vec{\mathbf{I}} \\
 -\phi p &= (Q \nabla \cdot \mathbf{s}_{sc} + R \nabla \cdot \mathbf{s}_{fc}).
 \end{aligned} \tag{141}$$

## 9.4 Compressional waves

### 9.4.1 Wave numbers

From Eq. (138) it can be seen that two compressional waves propagate. By taking the inverse of the matrix on the right-hand side, it can be written as

$$\nabla^2 \begin{bmatrix} \mathbf{s}_{sc} \\ \mathbf{s}_{fc} \end{bmatrix} = -\frac{\omega^2}{PR - Q^2} \begin{bmatrix} R\vec{\rho}_{11} - Q\vec{\rho}_{12} & R\vec{\rho}_{12} - Q\vec{\rho}_{22} \\ -Q\vec{\rho}_{11} + P\vec{\rho}_{12} & -Q\vec{\rho}_{12} + P\vec{\rho}_{22} \end{bmatrix} \cdot \begin{bmatrix} \mathbf{s}_{sc} \\ \mathbf{s}_{fc} \end{bmatrix}. \quad (142)$$

By writing

$$\nabla^2 \begin{bmatrix} \mathbf{s}_{sc} \\ \mathbf{s}_{fc} \end{bmatrix} = -\vec{\mathbf{k}}_{c1,2}^2 \cdot \begin{bmatrix} \mathbf{s}_{sc} \\ \mathbf{s}_{fc} \end{bmatrix} = -\frac{\omega^2}{PR - Q^2} \vec{\lambda}_{1,2} \cdot \begin{bmatrix} \mathbf{s}_{sc} \\ \mathbf{s}_{fc} \end{bmatrix}, \quad (143)$$

the eigenvalues  $\lambda_{1,2}$  can be obtained, with an isotropic medium, from

$$\det \begin{bmatrix} R\rho_{11} - Q\rho_{12} - \lambda_{1,2} & R\rho_{12} - Q\rho_{22} \\ -Q\rho_{11} + P\rho_{12} & -Q\rho_{12} + P\rho_{22} - \lambda_{1,2} \end{bmatrix} = 0. \quad (144)$$

This leads to wave numbers  $k_{c1,2}$  of the compressional waves obeying [20]

$$k_{c1,2}^2 = \frac{\omega^2}{PR - Q^2} \lambda_{1,2}, \quad (145)$$

where

$$\lambda_{1,2} = \frac{P\rho_{22} + R\rho_{11} - 2Q\rho_{12} \pm \sqrt{\Delta}}{2} \quad (146)$$

$$\Delta = (P\rho_{22} + R\rho_{11} - 2Q\rho_{12})^2 - 4(PR - Q^2)(\rho_{11}\rho_{22} - \rho_{12}^2).$$

With an anisotropic medium, the matrix corresponding that in Eq. (144) is

$$\begin{bmatrix} \vec{\mathbf{a}}_{11} & \vec{\mathbf{a}}_{12} \\ \vec{\mathbf{a}}_{21} & \vec{\mathbf{a}}_{22} \end{bmatrix} = \begin{bmatrix} R\vec{\rho}_{11} - Q\vec{\rho}_{12} - \vec{\lambda}_{1,2} & R\vec{\rho}_{12} - Q\vec{\rho}_{22} \\ -Q\vec{\rho}_{11} + P\vec{\rho}_{12} & -Q\vec{\rho}_{12} + P\vec{\rho}_{22} - \vec{\lambda}_{1,2} \end{bmatrix}. \quad (147)$$

The inverse of the matrix can be seen to be

$$\begin{bmatrix} \vec{\mathbf{a}}_{11} & \vec{\mathbf{a}}_{12} \\ \vec{\mathbf{a}}_{21} & \vec{\mathbf{a}}_{22} \end{bmatrix}^{-1} = \begin{bmatrix} \left( \vec{\mathbf{a}}_{11} - \vec{\mathbf{a}}_{12} \cdot \vec{\mathbf{a}}_{22}^{-1} \cdot \vec{\mathbf{a}}_{21} \right)^{-1} & -\vec{\mathbf{a}}_{11}^{-1} \cdot \vec{\mathbf{a}}_{12} \cdot \left( \vec{\mathbf{a}}_{22} - \vec{\mathbf{a}}_{21} \cdot \vec{\mathbf{a}}_{11}^{-1} \cdot \vec{\mathbf{a}}_{12} \right)^{-1} \\ -\vec{\mathbf{a}}_{22}^{-1} \cdot \vec{\mathbf{a}}_{21} \cdot \left( \vec{\mathbf{a}}_{11} - \vec{\mathbf{a}}_{12} \cdot \vec{\mathbf{a}}_{22}^{-1} \cdot \vec{\mathbf{a}}_{21} \right)^{-1} & \left( \vec{\mathbf{a}}_{22} - \vec{\mathbf{a}}_{21} \cdot \vec{\mathbf{a}}_{11}^{-1} \cdot \vec{\mathbf{a}}_{12} \right)^{-1} \end{bmatrix}. \quad (148)$$

By multiplying terms (1,1) and (2,1) in the right-hand side of Eq. (148) by

$$\left( \vec{\mathbf{a}}_{22} - \vec{\mathbf{a}}_{21} \cdot \vec{\mathbf{a}}_{11}^{-1} \cdot \vec{\mathbf{a}}_{12} \right) \cdot \left( \vec{\mathbf{a}}_{22} - \vec{\mathbf{a}}_{21} \cdot \vec{\mathbf{a}}_{11}^{-1} \cdot \vec{\mathbf{a}}_{12} \right)^{-1} = \hat{\mathbf{I}} \quad (149)$$

and terms (1,2) and (2,2) by

$$\left( \vec{\mathbf{a}}_{11} - \vec{\mathbf{a}}_{12} \cdot \vec{\mathbf{a}}_{22}^{-1} \cdot \vec{\mathbf{a}}_{21} \right) \cdot \left( \vec{\mathbf{a}}_{11} - \vec{\mathbf{a}}_{12} \cdot \vec{\mathbf{a}}_{22}^{-1} \cdot \vec{\mathbf{a}}_{21} \right)^{-1} = \hat{\mathbf{I}}, \quad (150)$$

we obtain

$$\begin{bmatrix} \vec{\mathbf{a}}_{11} & \vec{\mathbf{a}}_{12} \\ \vec{\mathbf{a}}_{21} & \vec{\mathbf{a}}_{22} \end{bmatrix}^{-1} = \begin{bmatrix} \left( \vec{\mathbf{a}}_{22} - \vec{\mathbf{a}}_{21} \cdot \vec{\mathbf{a}}_{11}^{-1} \cdot \vec{\mathbf{a}}_{12} \right) \cdot \vec{\mathbf{A}}^{-1} & -\vec{\mathbf{a}}_{11}^{-1} \cdot \vec{\mathbf{a}}_{12} \cdot \left( \vec{\mathbf{a}}_{11} - \vec{\mathbf{a}}_{12} \cdot \vec{\mathbf{a}}_{22}^{-1} \cdot \vec{\mathbf{a}}_{21} \right) \cdot \left( \vec{\mathbf{A}}^T \right)^{-1} \\ -\vec{\mathbf{a}}_{22}^{-1} \cdot \vec{\mathbf{a}}_{21} \cdot \left( \vec{\mathbf{a}}_{22} - \vec{\mathbf{a}}_{21} \cdot \vec{\mathbf{a}}_{11}^{-1} \cdot \vec{\mathbf{a}}_{12} \right) \cdot \vec{\mathbf{A}}^{-1} & \left( \vec{\mathbf{a}}_{11} - \vec{\mathbf{a}}_{12} \cdot \vec{\mathbf{a}}_{22}^{-1} \cdot \vec{\mathbf{a}}_{21} \right) \cdot \left( \vec{\mathbf{A}}^T \right)^{-1} \end{bmatrix} \quad (151)$$

where

$$\vec{\mathbf{A}} = \left( \vec{\mathbf{a}}_{11} - \vec{\mathbf{a}}_{12} \cdot \vec{\mathbf{a}}_{22}^{-1} \cdot \vec{\mathbf{a}}_{21} \right) \cdot \left( \vec{\mathbf{a}}_{22} - \vec{\mathbf{a}}_{21} \cdot \vec{\mathbf{a}}_{11}^{-1} \cdot \vec{\mathbf{a}}_{12} \right). \quad (152)$$

The eigenvalues  $\vec{\lambda}_{1,2}$  can now be obtained, instead of Eq. (144) or (146), from

$$\vec{\mathbf{A}} = 0 \quad (153)$$

and the corresponding wave numbers from

$$\vec{\mathbf{k}}_{c1,2}^2 = \frac{\omega^2}{PR - Q^2} \vec{\lambda}_{1,2} \quad (154)$$

or

$$k_{c1,2}^2 = \frac{\omega^2}{PR - Q^2} \mathbf{e}_1 \cdot \vec{\lambda}_{1,2} \cdot \mathbf{e}_1, \quad (155)$$

where  $\mathbf{e}_1$  is the propagation direction of the compressional wave.

#### 9.4.2 Displacement relationships

Combining Eqs. (138) and (143) we obtain

$$\omega^2 \begin{bmatrix} \vec{\rho}_{11} \cdot \mathbf{s}_{sc} & \vec{\rho}_{12} \cdot \mathbf{s}_{fc} \\ \vec{\rho}_{12} \cdot \mathbf{s}_{sc} & \vec{\rho}_{22} \cdot \mathbf{s}_{fc} \end{bmatrix} = \begin{bmatrix} P & Q \\ Q & R \end{bmatrix} k_{c1,2}^2 \begin{bmatrix} \mathbf{s}_{sc} \\ \mathbf{s}_{fc} \end{bmatrix}, \quad (156)$$

from which we get presentation for the displacement relationships between the compressional waves in the air and in the frame

$$\mathbf{s}_{fc} = \vec{\mu}_{1,2} \cdot \mathbf{s}_{sc}, \quad (157)$$

where quantity  $\vec{\mu}_{1,2}$  can be obtained from following alternative formulae

$$\begin{aligned}\vec{\mu}_{1,2} &= \left( \omega^2 \vec{\rho}_{12} - Qk_{c1,2}^2 \hat{\mathbf{I}} \right)^{-1} \cdot \left( Pk_{c1,2}^2 \hat{\mathbf{I}} - \omega^2 \vec{\rho}_{11} \right) \\ &= \left( \omega^2 \vec{\rho}_{22} - Rk_{c1,2}^2 \hat{\mathbf{I}} \right)^{-1} \cdot \left( Qk_{c1,2}^2 \hat{\mathbf{I}} - \omega^2 \vec{\rho}_{12} \right).\end{aligned}\quad (158)$$

### 9.4.3 Characteristic impedances

Four characteristic impedances can be defined, because both waves simultaneously propagate in the air and frame phases. The characteristic impedance  $Z_f$  and  $Z_s$  related to the propagation in the air and frame correspondingly are

$$\begin{aligned}Z_{fc} &= \frac{P}{j\omega \mathbf{s}_{fc} \cdot \mathbf{e}_1} \\ Z_{sc} &= -\frac{\mathbf{e}_1 \cdot \vec{\sigma}_{sc} \cdot \mathbf{e}_1}{j\omega \mathbf{s}_{sc} \cdot \mathbf{e}_1},\end{aligned}\quad (159)$$

where  $\mathbf{e}_1$  is a unit vector in the direction of propagation. Using Eqs. (141) these can be presented as

$$\begin{aligned}Z_{fc} &= -\frac{Q\nabla \cdot \mathbf{s}_{sc} + R\nabla \cdot \mathbf{s}_{fc}}{j\omega\phi \mathbf{s}_{fc} \cdot \mathbf{e}_1} \\ Z_{sc} &= -\frac{P\nabla \cdot \mathbf{s}_{sc} + Q\nabla \cdot \mathbf{s}_{fc}}{j\omega \mathbf{s}_{sc} \cdot \mathbf{e}_1}.\end{aligned}\quad (160)$$

By noting that

$$\nabla \cdot \mathbf{s} = -jks \cdot \mathbf{e}_1 \quad (161)$$

and utilizing Eq. (158), the impedances can be further presented as

$$\begin{aligned}Z_{fc1,2} &= k_{c1,2} \frac{Q\mathbf{e}_1 \cdot \vec{\mu}_{1,2}^{-1} \cdot \mathbf{s}_{fc} + R\mathbf{s}_{fc} \cdot \mathbf{e}_1}{\omega\phi \mathbf{s}_{fc} \cdot \mathbf{e}_1} \\ &= \frac{k_{c1,2}}{\omega\phi} \left( R + \frac{Q}{\mu_{12}} \right) \\ Z_{sc1,2} &= k_{c1,2} \frac{P\nabla \cdot \mathbf{s}_{sc} + Q\mathbf{e}_1 \cdot \vec{\mu}_{1,2}^{-1} \cdot \mathbf{s}_{sc}}{\omega \mathbf{s}_{sc} \cdot \mathbf{e}_1} \\ &= \frac{k_{c1,2}}{\omega} (P + \mu_{12}Q),\end{aligned}\quad (162)$$

where

$$\mu_{1,2} = \frac{\mathbf{e}_1 \cdot \vec{\mu}_{1,2}^{-1} \cdot \mathbf{s}_{sc}}{\mathbf{s}_{sc} \cdot \mathbf{e}_1} = \frac{\mathbf{s}_{fc} \cdot \mathbf{e}_1}{\mathbf{e}_1 \cdot \vec{\mu}_{1,2}^{-1} \cdot \mathbf{s}_{fc}}. \quad (163)$$



## 9.5 Shear waves

From Eq. (139) it can be seen that only one shear wave exists; the lower equation in (139) gives only the displacement relationship between the shear waves in the air and in the frame as

$$\mathbf{s}_{fs} = \vec{\boldsymbol{\mu}}_3 \cdot \mathbf{s}_{ss}, \quad (164)$$

where

$$\vec{\boldsymbol{\mu}}_3 = -\vec{\boldsymbol{\rho}}_{22}^{-1} \cdot \vec{\boldsymbol{\rho}}_{12}. \quad (165)$$

By inserting this to the first equation in Eq. (139) we obtain for the shear wave in the solid

$$-\omega^2 \left( \vec{\boldsymbol{\rho}}_{11} - \vec{\boldsymbol{\rho}}_{12} \cdot \vec{\boldsymbol{\rho}}_{22}^{-1} \cdot \vec{\boldsymbol{\rho}}_{12} \right) \cdot \mathbf{s}_{ss} = N \nabla^2 \mathbf{s}_{ss}. \quad (166)$$

By writing

$$\nabla^2 \hat{\mathbf{s}}_{ss} = -k_s \hat{\mathbf{s}}_{ss} \quad (167)$$

we obtain readily the wave number  $k_s$  of the shear wave

$$k_s^2 = \frac{\omega^2}{N} \left( \vec{\boldsymbol{\rho}}_{11} - \vec{\boldsymbol{\rho}}_{12} \cdot \vec{\boldsymbol{\rho}}_{22}^{-1} \cdot \vec{\boldsymbol{\rho}}_{12} \right). \quad (168)$$

## 10. Conclusions

---

Multi-scale asymptotic method (MAM) is a multi-scale approach based on an asymptotic analysis of the basic linearized equations of acoustics in the frequency domain. It is used to derive a set of well-posed micro-scale equations for computing effective macro-scale variables via averaging (homogenizing) over the unit cell. So the micro-scale properties are mapped to complex macro-scale parameters of equivalent fluids via homogenization. In setting the multi-scale equations it is supposed that the absorbing material under consideration can be handled as spatially periodic in the micro-scale. The material is thus assumed to include similar unit cells.

The macro-scale complex parameters can be defined using two alternative ways: the direct numerical approach and the hybrid numerical approach. The direct approach requires significant computation at each frequency. An alternative and lighter, analytic-based approach has been introduced recently, termed as the hybrid numerical approach. The absorption coefficients as a function of frequency, obtained from both approaches, are in very good agreement.

In the direct numerical approach, the dynamic Stokes and dynamic heat conduction problems in the dynamical multi-scale microstructural model are solved to obtain the dynamic micro-scale viscous and thermal permeability functions. The corresponding macro-scale dynamic permeabilities can be obtained by homogenization (averaging over the micro-scale). From these macro-scale permeabilities, the effective density and its normalized version dynamic viscous tortuosity, and the effective compressibility can be obtained. From these parameters, the impedance, the complex sound speed and the complex wave number for rigid frame models can be obtained.

In the hybrid numerical approach, the static Stokes and heat conduction problems in the static multi-scale microstructural model are solved to obtain the static micro-scale viscous and thermal permeability functions. The corresponding macro-scale static permeabilities can be obtained by homogenization (averaging over the micro-scale). From these macro-scale permeabilities, the viscous and thermal relaxed tortuosities can be obtained. The electrical conduction problem is solved to obtain the tortuosity and the viscous characteristic length. The thermal characteristic length is obtained from geometrical properties. From the parameters above, the dynamic viscous tortuosity and the normalized dynamic effective compressibility can be obtained. From these last parameters, the impedance, the complex sound speed and the complex wave number for rigid frame models can be obtained as in the direct approach.

The imaginary parts of the effective density and the effective compressibility are due to the viscous and thermal losses of the fluid in porous materials. The deviations of their real parts from their physical values take into account some other things affecting the sound propagation in porous materials, like isothermal behaviour at low frequencies and adiabatic at high frequencies, and the fact that sound cannot propagate in rectilinear motion due to the presence of the skeleton.

In the Biot model, the elastic behaviour of the frame is taken into account, leading to equations with three wave motions, two compressional waves and one shear wave, all of them propagating both in the air and the solid phase. The viscous and thermal effects are coupled, so the logic presented for the rigid frame models cannot be directly applied and the impedance, the complex sound speed and the complex wave number cannot now be obtained as done with the rigid frame models. However, the effective compressibility and the dynamic viscous tortuosity can directly be included in the parameters of the Biot model, to take into account the viscous and thermal properties of the fluid phase. The effective density and the effective compressibility, used in the Biot parameters, can be based on either the direct numerical approach or any of the methods in the hybrid numerical approach. The internal losses of the solid phase can be taken into account in a familiar way using complex elastic parameters of the viscoelastic structure.

According to simulation results in literature, there is a frequency dependent optimum of the radii of the fibres at constant porosity for maximum sound absorption. With constant porosity, decreasing the radius of the fibres implies an increase of the surface area of the fibres-pore interface, thus evidently increasing the viscous losses. However, if the radius is decreased too much, the range of the loss regions of two near-by fibres overlap and the viscous losses decrease. For larger fibres, the absorption coefficient is globally higher for a stimulation orthogonally to the lumens than along them. Smaller fibres absorb better the acoustic energy when stimulated along their internal porosity. Absorption coefficient globally increases when the material gets thicker. However, for each radius of the fibres at each frequency, there exists a critical thickness for which the asymptotic absorption coefficient is reached, and further increasing the thickness from this does not increase the absorption coefficient. Increasing the closure rate and decreasing the throat size from open-cell construction to an optimum value improves the middle frequency performance of absorptive foams. The cell size has an effect to the selectivity of the frequency band of high sound absorption. In sound insulation applications smaller closure rates are better.

## 11. Summary

---

The multi-scale computation method has been treated for acoustical purposes, for controlling the chain of parameters including the relations between the microscopic, macroscopic and acoustic parameters of sound absorbing materials. Possible anisotropic behaviour of materials has been taken into account.

The macro-scale parameters complex density and complex compressibility are produced by the multi-scale computation. Their imaginary parts are due to the viscous and thermal losses

of the fluid in porous materials. The deviations of their real parts from their physical values take into account some other things affecting the sound propagation in porous materials.

The macro-scale complex parameters can be defined using two alternative ways: the direct numerical approach and the hybrid numerical approach. In the former, the complex density and compressibility are directly formed from the calculated dynamic viscous and thermal permeability functions. In the latter, static viscous and thermal permeability functions, three tortuosity functions (the strict amount depending on the selection from three possible models), and the viscous and thermal characteristic lengths, are computed, from which the complex density and compressibility are finally calculated. From the complex density and compressibility, the impedance and the complex wave number for rigid frame models are computed similarly in both of the methods.

In the Biot model, the viscous and thermal effects are coupled, so the logic presented for the rigid frame models cannot be directly. However, the effective compressibility and the dynamic viscous tortuosity, based on either of the approaches, can directly be included in the parameters of the Biot model, to take into account the viscous and thermal properties of the fluid phase.

Some examples from literature have been given considering the optimization of the performance of the absorbing materials based on micro-scale modifications by the help on multi-scale computing.

## References

---

1. Delany, M. E. & Bazley, E. N., Acoustical properties of fibrous absorbent materials. *Appl. Ac.* 3 (1970), pp. 105–116.
2. Mechel, F. P., Ausweitung der Absorberformel von Delany und Bazley zu tiefen Frequenzen. *Acustica* 35(1976), pp. 210–213.
3. Va One 2012 Foam Module User's Guide, Theory & QA. ESI Group.
4. Bensoussan, A., Lions, J.-L. & Papanicolaou, G., *Asymptotic Analysis for Periodic Structures*. Amsterdam: North-Holland Publishing Company, 1978. 700 p.
5. Auriault, J.-L., Borne, L. & Chambon, R., Dynamics of porous saturated media, checking of the generalized law of Darcy. *J. Acoust. Soc. Am.* 77(1985)5, pp.1641–1650.
6. Boutin, C., Royer, P. & Auriault, J. L., Acoustic absorption of porous surfacing with dual porosity. *Int. J. Solid Structures* 35(1998)34–35, pp. 4709–4737.
7. Lafarge, D., Lemarinier, P., Allard, J. F. & Tarnow, V., Dynamic compressibility of air in porous structures at audible frequencies. *J. Acoust. Soc. Am.* 102(1997)4, pp. 1995–2006.
8. Lee, C.-Y. & Leamy, M. J., Acoustic absorption calculation in irreducible porous media: A unified computational approach. *J. Acoust. Soc. Am.* 126(2009)4, pp. 1862–1870.
9. Lafarge, D., The equivalent fluid model. In: Bruneau, M. & Potel, C. (editors), *Materials and Acoustic Handbook*. London: ISTE Ltd., 2009. 919 p.
10. Perrot, C., Chevillotte, F. & Panneton, R., Dynamic viscous permeability of an open-cell aluminium foam: Computation versus experiments. *J. Appl. Phys.* 103(2008), 024909.
11. Perrot, C., Chevillotte, F. & Panneton, R., Bottom-up approach for microstructure optimization of sound absorbing materials. *J. Acoust. Soc. Am.* 124(2008)2, pp. 940–948.
12. Lee, C.-Y., Leamy, M. J. & Nadler, J. H., Frequency band structure and absorption predictions for multi-periodic acoustic composites. *J. Sound Vib.* 329(2010), pp. 1809–1822.
13. Duval, A., Hoang, M. T., Marcel, V. & Perrot, C., Development of acoustically effective foams: a new micro-macro optimization method. *VDI Pur Tagung* 2012.
14. Peyrega, C. & Jeulin, D., Effects of the microstructure of fibrous media on their acoustic properties. *Proceedings of the COMSOL Conference 2010, Paris*.
15. Peyrega, C. & Jeulin, D., Estimation of acoustic properties and of the representative volume element of random fibrous media. *J. Appl. Phys.* 113(2013)10491.

16. Uosukainen, S., Acoustic field theory. Espoo: Aalto University, Science + Technology 17/2013, 2013. 633 p. In Finnish.
17. Hoang, M. T. & Perrot, C., Solid films and transports in cellular foams. *J. Appl. Phys.* 112(2012), 054911.
18. Temkin, S., *Elements of Acoustic*. New York: John Wiley & Sons, 1981. 515 p.
19. Johnson, D. L., Koplik, J. & Dashen, R., Theory of dynamic permeability and tortuosity in fluid-saturated porous media. *J. Fluid Mech.* 176(1987), pp. 379–402.
20. Allard, J. F. & Atalla, N., *Propagation of Sound in Porous Media*. Chichester: John Wiley & Sons, 2009. 358 p.
21. Perrot, C., Chevillotte, F., Hoang, M. T., Bonnet, G., Bécot, F.-X., Gautron, L. & Duval, A., Microstructure, transport, and acoustic properties of open-cell foam samples: Experiments and three-dimensional numerical simulation. *J. Appl. Phys.* 111(2012), 014911.
22. Pride, S. R., Morgan, F. D. & Gangi, A. F., Drag forces of porous medium acoustics. *Phys. Rev. B* 47(1993), pp.4964–4978.
23. Lafarge, D., *Propagation du son dans les matériaux poreux à structure rigide saturés par un fluide viscothermique*. Ph.D. thesis, Université du Maine, 1993.
24. Champoux, Y. & Allard, J. F., Dynamic tortuosity and bulk modulus in air-saturated porous media. *J. Appl. Phys.* 70(1991), 1975.